Glaciomarine sequence stratigraphy in the Mississippian Río Blanco Basin, Argentina, southwestern Gondwana. Basin analysis and palaeoclimatic implications for the Late Paleozoic Ice Age during the Tournaisian.

Miguel Ezpeleta[1,2]*, Juan José Rustán[1,2], Diego Balseiro[1], Federico Miguel Dávila[1], Juan Andrés Dahlquist[1], Norberto Emilio Vaccari[1,2], Andrea Fabiana Sterren[1], Cyrille Prestianni[3], Gabriela Adriana Cisterna[1,2] and Miguel Basei[4]

[1] CICTERRA-CONICET, Universidad Nacional de Córdoba, Av. Haya de la Torre s/n, X5015GCA, Córdoba, Argentina
[2] Universidad Nacional de La Rioja, Av. Luis M. de la Fuente s/n, F5300, La Rioja, Argentina
[3] Palaeontology Department, Royal Belgian Institute of Natural Sciences, Rue Vautier 29, 1000 Brussels, Belgium
[4] Instituto de Geociências, Universidade de São Paulo, São Paulo, Brazil

ME, 0000-0002-7188-7169; DB, 0000-0003-3015-9066; MB, 0000-0002-3857-7089
* Correspondence: miguelezpeleta@gmail.com

Abstract: The Late Paleozoic Ice Age (LPIA) has been well recorded in the uppermost Mississippian–Pennsylvanian of Gondwana. Nevertheless, little is known about the temporal and geographic dynamics, particularly during the early Mississippian. We report on exceptional Tournaisian glaciomarine stratigraphic sections from central Argentina (Río Blanco Basin). Encompassing *c.* 1400 m, these successions contain conspicuous glacigenic strata with age constraints provided by palaeontological data and U/Pb detrital zircon age spectra. A variety of marine, glaciomarine and fan-deltaic environments indicate relative sea-level variations mainly associated with tectonism and repetitive cycles of glacial activity. Provenance analysis indicates a source from the Sierras Pampeanas basement located to the east. Fifteen sequences were grouped into three depositional models: (1) Transgressive Systems Tracts (TST) to Highstand Systems Tracts (HST) sequences unaffected by glacial ice; (2) Lowstand Systems Tracts (LST) to TST and then to HST with glacial influence; and (3) non-glacial Falling-Stage Systems Tracts (FSST) to TST and HST. The glacial evidence indicates that the oldest Mississippian glacial stage of the LPIA in southwestern Gondwana is constrained to the middle Tournaisian. In contrast with previous descriptions of Gondwanan coeval glacial records, our sequence analysis confirms complex hierarchical climate variability, rather than a single episode of ice advance and retreat.

Supplementary material: Detailed stratigraphic sections, palaeocurrents and compositional analysis and U/Pb detrital Zr methodology and data are available at: https://doi.org/10.6084/m9.figshare.c.5011424

Received 23 December 2019; **revised** 5 June 2020; **accepted** 5 June 2020

The Late Paleozoic stratigraphic records of South America offer clues in the attempt to unravel the puzzle of palaeoclimatic and tectono-sedimentary processes that have been classically acknowledged as a hallmark of Gondwana. The onset of glacial influence in Gondwana has been recognized since the Late Devonian (Caputo *et al.* 2008; Montañez and Poulsen 2013), with noticeable records even at low palaeolatitudes of the Appalachian region, outside Gondwana (Brezinski *et al.* 2010, 2008). In contrast to earlier models suggesting a single and protracted glaciation stage (Veevers and Powell 1987), current evidence supports a complex pattern of alternating intervals with and without evidence of glaciation (Fielding *et al.* 2008a), superimposed onto a long-term pattern of climate change from ice-house conditions during the Carboniferous, up to warm-temperature, arid environments in the Permian (Montañez and Poulsen 2013). This palaeoclimatic trend is partially recorded in the foreland areas to intracratonic basins in South America and has been nourished by sedimentology, stratigraphy, palaeontology and isotopic geology (Gulbranson *et al.* 2010, 2014; Limarino *et al.* 2014; Pazos *et al.* 2017).

From a stratigraphic point of view, great effort has been spent on correlating and temporally organizing the different Gondwanan glacial/eustatic horizons occasionally obscured by tectonic deformations (Limarino *et al.* 2014). In the Andean context of South America, a revised Carboniferous chronostratigraphic scheme based on western Argentinian basins shows diachronous alpine and continental glaciations (Gulbranson *et al.* 2010; Limarino *et al.* 2014). However, some critical intervals, such as the lowermost Carboniferous, are still poorly understood and strongly debated. This is partially due to the lack of complete and well-developed stratigraphic records and specific studies. The regional apex of the Gondwanan glaciation during the Pennsylvanian eroded most of the underlying Mississippian rocks in South America to different degrees, leaving a scarce and patchy stratigraphic record. Based on this limited evidence, a middle Tournaisian and a middle Visean glaciation have been suggested as the oldest Mississippian glacial events in Gondwana (Caputo *et al.* 2008; Lakin *et al.* 2016). In the last decade, the middle Visean glaciation has been widely recognized in outcrops and subsurface foreland areas and intracratonic basins, especially in South America (Caputo *et al.* 2008; Gulbranson *et al.* 2010; Rosa *et al.* 2019). However, the Tournaisian glaciation is still highly controversial. Evidence is scarce and is mainly derived from the subsurface (Caputo *et al.* 2008; Lakin *et al.* 2016), while revisions based on described outcrops lack virtually any record of glacial activity (López Gamundí *et al.* 1992; Niemeyer *et al.* 1997; Limarino *et al.* 2014), despite some pre-Visean glacial

evidence from Argentina, mainly from the Precordillera (Pazos 2007) and central-western Patagonia (Taboada *et al.* 2019). In turn, some glacial records formerly considered as possibly lower Tournaisian have recently been re-assigned to the Strunian, the uppermost Devonian (e.g. Wicander *et al.* 2011). This might indicate an important gap in the LPIA record across western Gondwana, particularly during the lowermost Mississippian. Such a limited ice-proximal record hinders our understanding of Tournaisian climate and puts into question the nature and origin of pervasive ice-distal isotopic records (Yao *et al.* 2015).

In this contribution, we analyse a very thick Tournaisian siliciclastic marine succession in the Río Blanco Basin, exposed at Sierra de Las Minitas, western Argentina, south-central Andes (see Fig. 1). With *c.* 1400 m thick, this succession constitutes the first compelling evidence of glaciomarine lower Mississippian outcropping in South America, and at the same time the most significant record for the Tournaisian of this region. In addition to the interpretation of the tectono-stratigraphic development of the basin, this study allows us to improve our understanding of the earliest stages of the LPIA in southwestern Gondwana by filling in the above-mentioned stratigraphic gap. For local and regional correlations, we dealt with available biostratigraphic schemes (e.g. Limarino *et al.* 2014; Carrizo and Azcuy 2015), whereas the basin provenance was addressed using detrital zircon ages. Our work combines different data sets (stratigraphic, palaeontological and geochronological) in order to assemble a logical sequence stratigraphic framework. All this information allows us to interpret the tectonostratigraphic setting of the basin and, in particular, the stratigraphic record indicating relative sea-level changes (i.e. climatic v. tectonic controls) and their significance for the initial development of the LPIA in western Gondwana.

Geological setting

For decades, the Mississippian geological history of southwestern Gondwana, particularly in western Argentina, has been intensely debated from palaeogeographic, palaeoclimatic, basin evolution and tectonic and geodynamic scenarios (e.g. Limarino and Césari 1993; López Gamundí *et al.* 1994; Fernández-Seveso and Tankard 1995). However, there has recently been some consensus on associating it with regional extension to transtension along the margin (based on basin analysis: Fernández-Seveso and Tankard 1995; Astini *et al.* 2009, 2011; Ezpeleta 2009; Milana and Di Pasquo 2019; volcanic geochemistry: Báez *et al.* 2014; Coira *et al.* 2016; and structural and geochemistry analysis of basic dykes: Martina *et al.* 2018). Other contributions, mainly based on studies of Upper Devonian–Mississippian calc-alkaline and A-type granites (Dahlquist *et al.* 2013), have suggested alternations of compression and extension (tectonic switching model, cf. Collins 2002) as a consequence of episodic changes of the subduction angle.

The Mississippian record exposed at Sierra de Las Minitas (Fig. 1) corresponds to the proto-Andean Río Blanco Basin (Limarino and Spalletti 2006), west-central Argentina. Of the western Argentinian Mississippian proto-Andean basins, the Río Blanco Basin (Amos 1964) is the most northern, while the Calingasta-Uspallata basin is located further south. However, both basins have also been considered as depocentres of a single larger basin, the Uspallata-Iglesia Basin (González 1985; Carrizo and Azcuy 2015). To the east, the Río Blanco Basin exhibits complex magmatism and a noticeable variability in subsidence and sedimentation rates (e.g. Báez *et al.* 2014). These depocentres developed at a very high, southern latitudinal position (see Carrizo and Azcuy 2015), but the tectonically driven stratigraphic patterns hinder the interpretation and correlation of the climatic stratigraphic signal, usually including ice influence. The Mississippian deposits in the Río Blanco Basin have been attracting attention since the mid-twentieth century, but the main

focus has been on the southern part of the basin, while northern regions have been poorly addressed (e.g. Borrello 1955; Scalabrini Ortiz and Arrondo 1973; González and Bossi 1986; Fauqué and Limarino 1991; Coughlin 2000; Gutiérrez and Limarino 2006; Ezpeleta and Astini 2008; Astini *et al.* 2011; Carrizo and Azcuy 2015; Prestianni *et al.* 2015, among others).

The structural style of the Sierra de Las Minitas is characterized by basement thrusts that displace metamorphic and igneous lower Paleozoic rocks (western Sierras Pampeanas) onto Upper Paleozoic, Mesozoic and Cenozoic units. The mid-upper Paleozoic units developed localized low-grade metamorphism and intense folding, and are intruded by uppermost Devonian to Mississippian igneous dikes (Ar–Ar ages, *c.* 346–364 Ma, Coughlin 2000). Evidence of these Paleozoic deformations can also be seen in the different stratigraphic truncations and angular unconformities which separate the transgressive–regressive marine successions described below (Coughlin 2000; Astini *et al.* 2005; Ezpeleta 2009).

On a regional scale, Mississippian stratigraphic units outcropping at Sierra de Las Minitas have traditionally been correlated with units from the Angualasto Group (which originally included the Malimán and Cortaderas formations in the type section, Limarino and Césari 1993), exposed further south in San Juan province (Río Blanco and Calingasta-Uspallata basins). Figure 2 summarizes the different local to regional lithostratigraphic nomenclatures previously used (e.g. Limarino *et al.* 2006, 2017). The bulk of the Mississippian record from Sierra de Las Minitas was originally referred to the poorly defined Jagüel Formation (González and Bossi 1986), attributed to the Mississippian *sensu lato* (Fauqué and Limarino 1991). Although the use of this formational name has persisted in the literature (e.g. Gulbranson *et al.* 2010), Carrizo and Azcuy (1998, 2015) argued that it is devoid of any stratigraphic meaning and is therefore invalid and should be abandoned. An updated stratigraphic scheme for this region was provided by Azcuy *et al.* (1999) and Carrizo and Azcuy (2015). Three main Mississippian units can be identified in the study area, from the base to the top: (1) the Tournaisian Agua de Lucho Formation, mainly composed of shales and sandstones interbedded with glacial diamictites; (2) the Visean Cerro Tres Cóndores Formation, essentially formed of sandstones and thick polymictic conglomerates, some indicating the presence of ice; and (3) the Visean Punta del Agua Formation, consisting of coarse volcano-sedimentary deposits interbedded with glacial diamictites. The Pennsylvanian Río del Peñón Formation unconformably covers these Mississippian successions and also the lower to middle Devonian successions that are attributed to the Talacasto and Chigua formations (Rustán *et al.* 2011; Carrizo and Azcuy 2015).

In the southwestern area of Sierra de Las Minitas, the stratigraphic units are exposed along a slightly NE-plunging and east-vergent asymmetrical syncline, known as the Agua Quemada syncline (Fig. 1). The Agua de Lucho and Cerro Tres Cóndores formations show a continuous exposure *c.* 1400 m thick in this area. We studied two detailed stratigraphic sections separated by 2.5 km (Supplementary Material 1). The base of the Agua de Lucho Formation is not exposed since it is in tectonic contact with younger, folded Mississippian successions, while the upper limit is represented by a progressive, concordant passage to conglomeratic successions in the Cerro Tres Cóndores Formation. In these outcrops, the top of the Cerro Tres Cóndores Formation is eroded, and only 200 m are preserved.

It is worth mentioning that the glacial diamictites reported by Fauqué and Limarino (1991) and Limarino *et al.* (2017) in this area are not the same as those that we describe here for the Agua de Lucho Formation. Diamictites previously recognized by these authors crop out in a different tectonic block towards the NW and, based on our field observations, probably belong to a different, undescribed, younger stratigraphic unit.
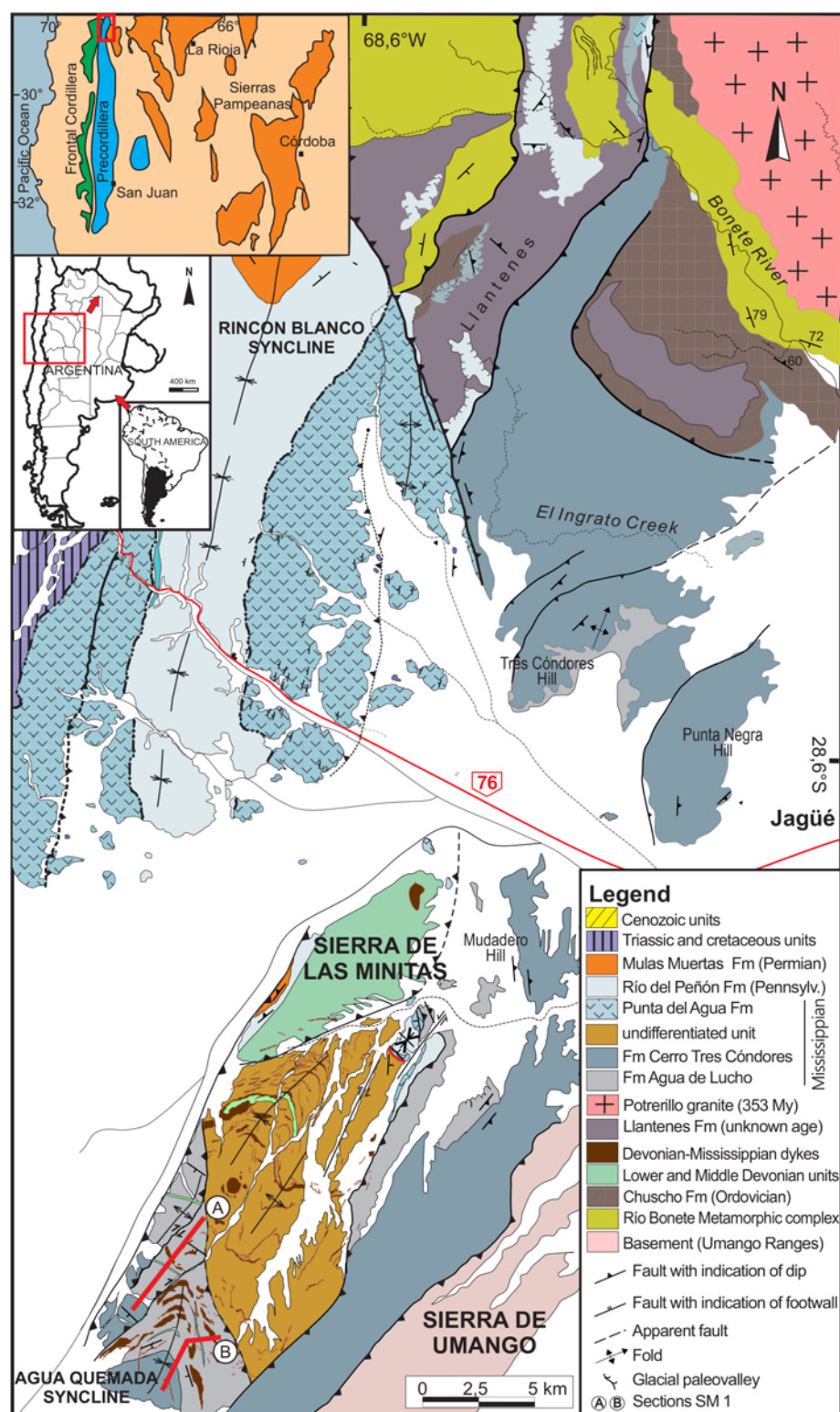
Fig. 1. Location map and regional geological information of the studied area: Sierra de Las Minitas northern Precordillera, north-west of La Rioja Province, Argentina. A and B are the two sections studied in this work (Supplementary Material 1).

Palaeontological content and age constraints

The sedimentary successions studied contain a rich fossiliferous record, mainly represented by marine invertebrates and plants. Fossil assemblages are usually dominated by brachiopods and bivalves (González 1994; Sterren et al. 2013), with subordinate crinoids, cephalopods, gastropods, hyoliths, conulariids and corals. Scarce records of bryozoans, fishes, sponges (Carrera et al. 2018) and trilobites (Vaccari et al. 2013) are restricted to a few specific intervals (Fig. 3 and Supplementary Materials 1). Plant remains have been studied by Azcuy and Carrizo (1995); Carrizo and Azcuy (1998, 2015) and Prestianni et al. (2015).

Deposits herein assigned to the Agua de Lucho Formation are considered Tournaisian in age due to the occurrence of the index miospore *Waltzispora lanzonii* (Daemon 1974), studied by Prestianni et al. (2015). This index spore was reported about 50 m above the base of the uppermost diamictite bed in the Agua Quemada syncline (S6 in Fig. 3 and Supplementary Materials 1) and probably supports a middle to late Tournaisian age for the bearing layers (but see Playford and Melo 2010; Lakin et al. 2016). There is no evidence for Devonian sediments in the Agua de Lucho Formation in this locality, and preliminary palynological reports suggesting such an age are currently considered reworked material (see Prestianni et al. 2015).
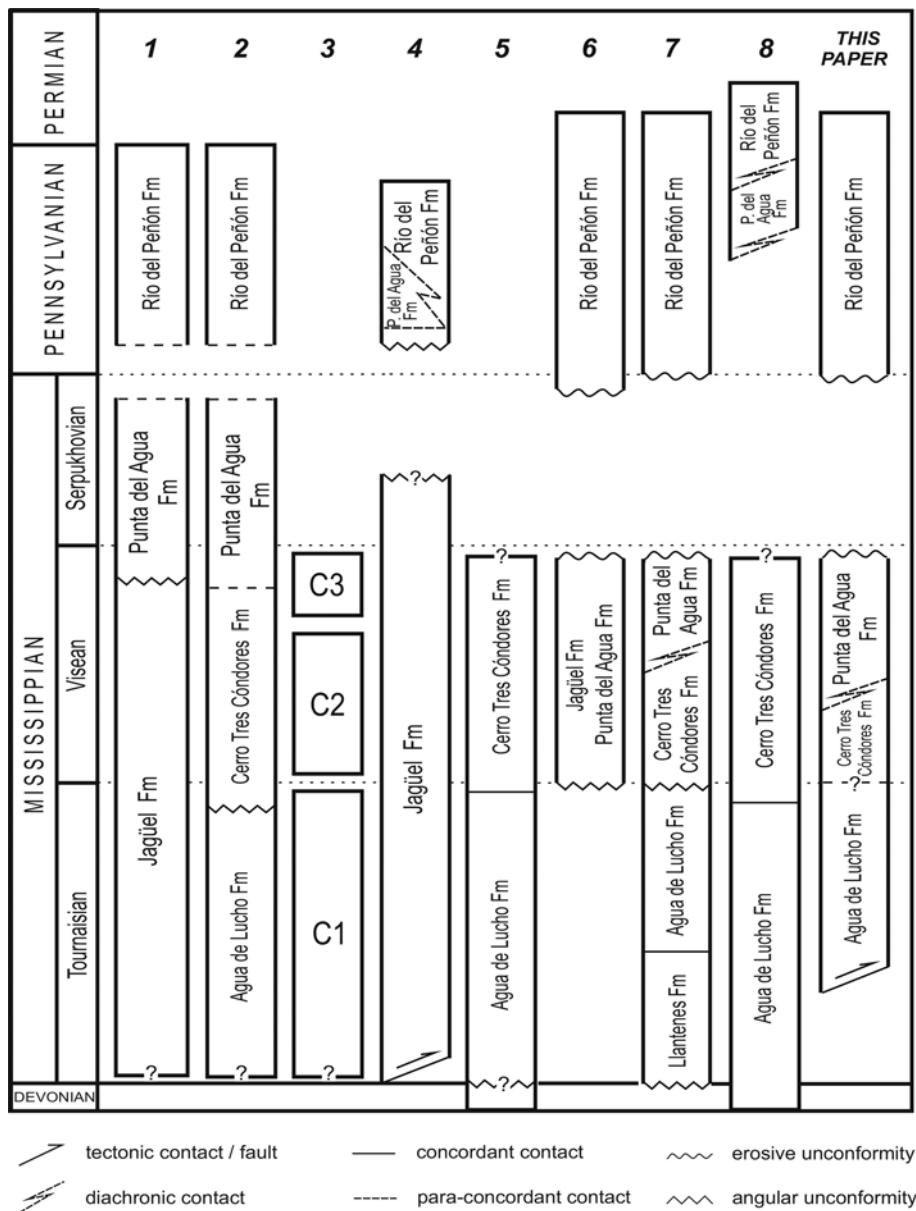
Fig. 2. Chronostratigraphy of the Río Blanco Basin. Columns 1 to 8 document the established stratigraphy by previous authors and the far-right column represents the redefined stratigraphy presented here. (**1**) González and Bossi (1986), (**2**) González and Bossi (1987), (**3**) Caminos *et al.* (1990), (**4**) Fauqué and Limarino (1991), (**5**) Carrizo and Azcuy (1998), (**6**) Gulbranson *et al.* (2010), (**7**) Astini *et al.* (2011) and Báez *et al.* (2014), (**8**) Carrizo and Azcuy (2015).

Records of the brachiopod *Azurduya chavelensis* (Amos) below and above the level yielding *W. lanzonii* (Sterren *et al.* 2013) support a Tournaisian age for the whole section of the Agua de Lucho Formation. *Azurduya* is a key element of the probably late Tournaisian *Michiganites scalabrinii-Azurduya chavelensis* zone (Sabattini *et al.* 2001), defined in the Malimán Formation (further south of the studied region) and recorded in other coeval southwestern Gondwanan basins (Niemeyer *et al.* 1997; Isaacson and Dutro 1999; Cisterna and Isaacson 2003; Sterren and Cisterna 2010; Cisterna 2011; Rubinstein *et al.* 2017).

The Cerro Tres Cóndores Formation has been considered as Visean by Carrizo and Azcuy (2015) based on plant assemblages attributed to the *Frenguellia-Paulophyton* zone. This unit underlies the volcaniclastic Punta del Agua Formation, which is dated at 336–337 myr (Gulbranson *et al.* 2010; Báez *et al.* 2014).

Methodology

Facies analysis and palaeoenvironmental interpretation

Fieldwork observations consisted of the recognition of lithology, texture, colour, fabric and sedimentary structures, and a description of the fossil content. The smaller-scale architectural elements and fabric (metrics) were defined according to the terms outlined by Dalrymple *et al.* (2012) and Fielding (2018), while larger-scale geometries (10–100 m) were analysed according to the characteristics defined by DeCelles *et al.* (1991) and McCarthy and Plint (1998).

Sequence stratigraphy

We interpreted the vertical and lateral variation of facies associations following Catuneanu (2017) and Catuneanu *et al.* (2011, 2009). This allowed us to interpret not only the different types of sequence boundaries and sequences, but also their relative depositional systems tracts. It is important to note that the sequence stratigraphy terminology has been proposed for low-latitude sequences and, therefore, might not be suitable to describe high-latitude glacial-influenced deposits. Considering that the studied area shows recurrent glacial records, particularly in the lower section, we also followed the Fielding (2018) sequence stratigraphic model, proposed mainly for glacial environments. This sequence stratigraphy model is essentially an adaption of the classical sequence stratigraphic approaches to glacial systems (e.g. Catuneanu *et al.* 2009).
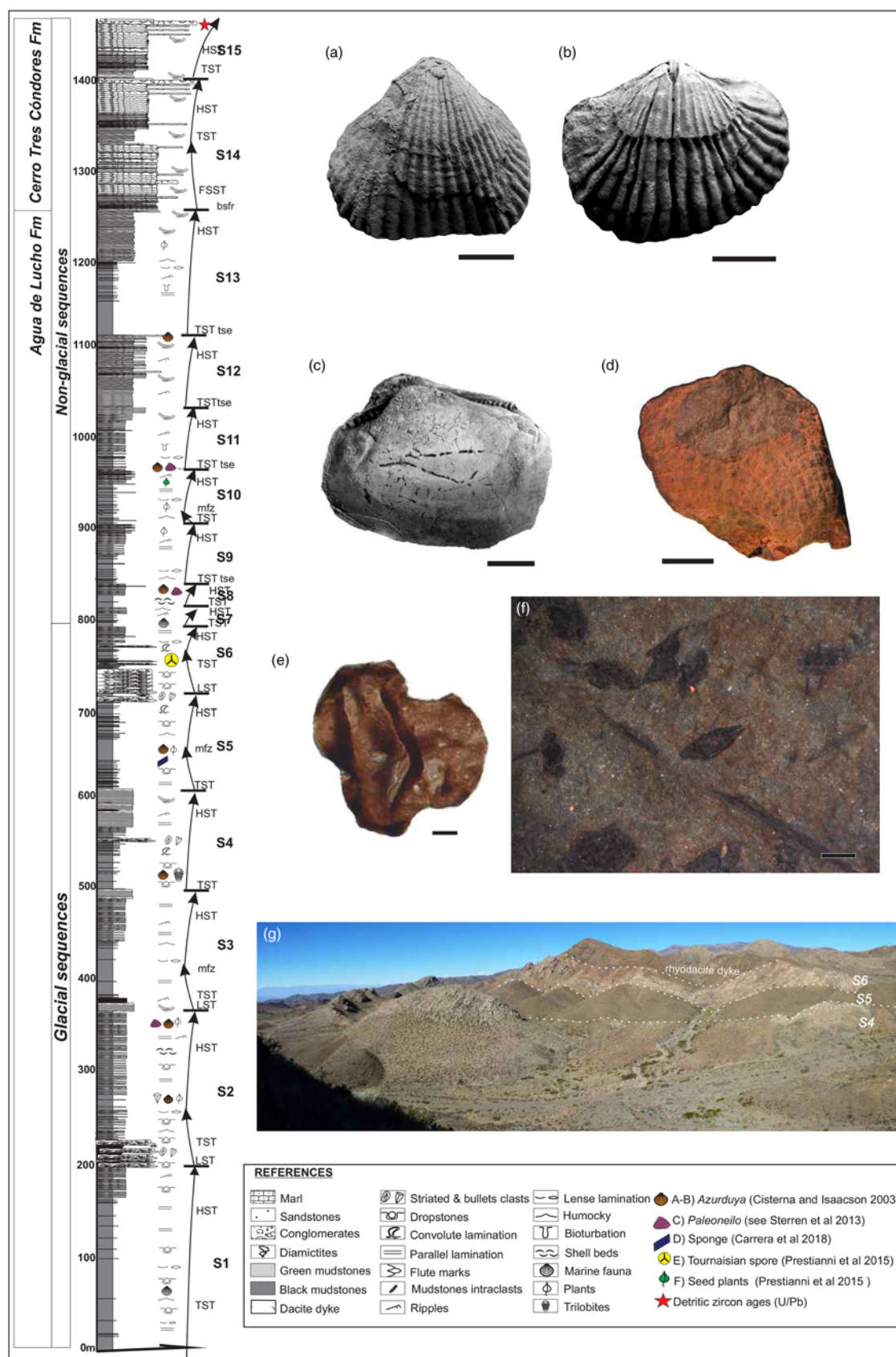
Fig. 3. Synthetic stratigraphic section and palaeontological content of southern Sierra de Las Minitas (for more details of facies and palaeoenvironmental interpretation see Tables 1 and 2, and Supplementary Material 1). S1 to S15, number of sequences (see below). LST, lowstand systems tract; TST, transgressive systems tract; HST, highstand systems tract; FSST, falling-stage systems tract; BSFR, basal surface of forced regression; MFS, maximum flooding surface; TSE, transgressive surface of erosion. (**a**) and (**b**) the Tournaisian-Visean South American brachiopod Azurduya chavelensis (Amos, 1958). PULR-I 7; PULR-I 8; Scale bar = 5 mm. (**c**) the common bivalve Palaeoneilo subquadratum (González, 1994), PULR-I 6 Scale bar = 5 mm. (**d**) the sponge Minitaspongia parvis (Carrera *et al.* 2018) PULR-I 4 Scale bar = 10 mm. (**e**) the Tournaisian index miospore Waltzispora lanzonii (Prestianni *et al.* 2015, Daemon 1974) PULR-166, Scale bar = 5 μm and (**f**) the oldest seed records from western Gondwana, Warsteinia sancheziae (Prestianni *et al.* 2015) and Pseudosporogonites cf. hallei (Stockmans), as reported by Prestianni *et al.* (2015). (**g**) Panoramic photo of sequences 4, 5 and 6.

Provenance

The provenance analysis was based on a compositional analysis of gravel in conglomerates, sandy matrix in gravelly beds and sandstones (Howard 1993). We also used palaeocurrent data to interpret the location of potential source areas (cf. Potter and Pettijohn 1977; DeCelles *et al.* 1983). The palaeocurrent directions were computed using rose diagrams in Stereonet software (Cardozo and Allmendinger 2013). Conglomerate composition and palaeocurrent measurements and their statistical analyses are available in Supplementary Material 2. This stratigraphic methodology of provenance analysis was carried out on different outcrops of the Sierra de Las Minitas and nearby hills. At the top of the Cerro Tres Cóndores Formation in southern Sierra Las Minitas, we complemented sedimentological techniques with U–Pb detrital zircon dating (see geochronological methodology in Supplementary Material 3 for further details).

Facies analysis, sequence stratigraphy and provenance

Facies analysis and palaeoenvironmental interpretation

For the study region (see Fig. 1 for location), we described and interpreted 16 lithofacies and seven facies associations (see details in Tables 1 and 2, Fig. 4 and 5). Figure 3 and Supplementary Material 1 show the vertical distribution of facies and facies associations; together with the facies analysis, this information helped us to analyse the sequence stratigraphy.

The Agua de Lucho Formation and the basal successions of the Cerro Tres Cóndores Formation contain a high-resolution record which can be used to reconstruct the depositional processes and palaeoenvironment of a highly complex glaciomarine setting, driven by autocyclic and allocyclic controls. The vertical succession and geometry of the depositional units allow the reconstruction of a complex facies mosaic for the basal interval, where glacial influence is observed (800 m in section A and 230 m in section B, see Supplementary Materials 1). The proximal glaciomarine environment is characterized by mass flow deposits and subaqueous channels in a fan delta, deposited by low-temperature, highly sediment-laden underflows (see FA A in Table 2) with subsequent wave reworking in a shoreface (FA B). Closely associated with the proximal glaciomarine environment are proglacial deltaic deposits and rhythmites (FA C). Siltstones and mudstones with sandy beds indicate suspension which is cyclically interrupted by tractive currents (cf. Dalrymple *et al.* 2012). Locally, intervals with dropstones suggest a floating ice sheet (Fig. 6). The influence of icebergs is more pronounced in the distal glaciomarine environment (outer to inner shelf). Distal glaciomarine deposits include subtidal channels with glacial features (FA D). Shallowing-upward successions develop from the outer-shelf to shoreface profile (FA E, F and G) after glacial retreat. These coastal deposits are then overridden by the next glacial advance. The evidence of variations in meltwater streams and short-term advances and retreats of the ice front suggest temperate glaciers (cf. Powell and Cooper 2002; Fielding 2018).

The facies associations present in the upper successions of the Agua de Lucho Formation (from 800 to 1260 m in section A, and 230 to 730 m in section B) suggest that this interval was deposited in a shallow coastal environment without glacial influence. It is a repetitive coastal-deltaic or shelf-margin progradation, from outer–inner shelf (FA C) to shoreface facies association (FA E, F and G).

The deposition of the Cerro Tres Cóndores Formation is represented by an abrupt coarsening-upward succession that is interpreted as a shallow water to shelf-type fan delta (Lønne 1995, see FA G and H in Table 2). Internally, this unit shows moderate fluctuation in relative sea-level as suggested by the intermittence of fluviatile to shoreface conditions.

Sequence stratigraphy

Vertical and lateral variation of facies associations (FA) allow us to define, describe and interpret different types of sequence boundaries and depositional systems tracts. Figure 3 illustrates the 15 stratigraphic sequences defined in this work, internally divided into different systems tracts (see details in Supplementary Materials 1).

Even though successive sequences may preserve slightly different combinations of facies and facies associations, there is rather good consistency in the facies composition of sequences, and an idealized sequence or motif can be deduced (cf. Fielding 2018). The subaqueous channels (FA A) and shoreface proximal to ice front deposits (FA B) were interpreted as Lowstand Systems Tracts (LST) during glacial maximum. Fining-upward succession dominated by sandy levels with occasional subtidal channels (FA D) represents Transgressive Systems Tract (TST) deposits or glacial retreat, and fine-grained facies (FA C) indicate a glacial minimum or maximum flooding zone (MFZ). The shoreface facies associations E, F and G indicate marine to coastal shallowing-upward successions, which are typical elements of Highstand Systems Tracts (HST). Locally, these HST present glacial features suggesting episodic glacial advances. It is important to note that Falling Stage Systems Tract (FSST) deposits, represented by subaerial to shallow water fan deltas (FA G and H), develop above basal forced regression surfaces (BSFR), particularly when Lowstand Systems Tracts (LST) are poorly represented.

Each stratigraphic sequence, from bottom to top, is described below (see details in Supplementary Materials 1). The basal boundary is not recorded and lower section of Sequence 1 (S1, *c.* 200 m thick) is partially recorded. S1 is tectonically deformed and covered by younger deposits, so its thickness is approximated. The preserved fine-grained basal deposits (FA C) represent a TST, where numerous dropstones suggest a glacial minimum. This succession is followed by shoreface deposits (FA E, F and G) without glacial records, representing an HST. This monotonous interval >100 m thick indicates relative sea-level stability as aggradation dominates over progradation.

The erosive base of Sequence 2 (S2, *c.* 170 m thick) is defined at a point, where there is an abrupt upwards transition from fine- to coarse-grained lithologies. This surface is interpreted as a glacial surface of erosion. Facies directly overlying the sequence boundary are the coarsest in the sequence and represent the LST. Diamictites are interbedded with conglomerates and sandstones (FA A) fining upwards to sandstones with dropstones (FA B), and are interpreted as a glacial advance stage followed by a period of ice retraction. Overlying these facies develop thin, fine-grained bioturbated siltstones (FA C) that represent the MFZ. Mudrocks coarsen upwards into a sandstone-dominated interval showing extensive preservation of current and wave-generated sedimentary structures containing several levels with marine invertebrate and plant fossils (Fig. 3 and Supplementary Materials 1). The lower to middle shoreface deposits (FA E and F) suggest a shallowing-upward progradation during an HST stage, and dropstones at the base of this interval would indicate a contemporary glacial advance.

Sequence 3 (S3, *c.* 130 m thick) starts with an erosive surface and shows an arrangement similar to S2, but without (or poor) evidences of glacial features. Above the basal erosive surface are thick, coarse sandstone beds with trough cross-bedding, interpreted as upper shoreface facies without glacial facies (FA G) and representing the LST. This coarser interval is overlain by a thin fining-upward succession dominated locally by pelitic successions with scattered dropstones (FA C), and is interpreted as the final stage of the TST during glacial retreat. A prograding shallowing-upward trend is indicated by a transition from mid-shelf to shoreface facies (FA F and G). A monotonous shoreface succession up section suggests aggradation during a relatively stable HST stage.

Table 1. *Summary of lithofacies recognized in southern Sierra de Las Minitas, with process interpretations. Lithofacies classification scheme (after Miall 1996). In the second column are the photographs corresponding to each facies (Figs 4 and 5)*

	Facies	Description	Interpretation of processes
1	Fl (Fig. 4a)	Laminated to massive green to black mudstones (1–10 cm thick). Stringers of coarser-grained sands are common. Slightly wavy lamination is sometimes present. Extraformational **dropstones** (granitic, metamorphic and limestones) of 1–15 cm and intense bioturbation are common.	Deposition from suspension or low energy currents (Bann and Fielding 2004; MacEachern and Bann 2008). Dropstones represent supply of clasts from **ice rafting**.
2	Fl + Sr (Figs 4b and 6a and b)	Intervals of 1–10 m of interstratified mudstones, siltstones and very fine yellowish tabular sandstones (2–5 cm thick). Bioturbation and ripple structures are common. Intense **soft-sediment deformation** interbedded between non-deformed horizons are frequent. **Dropstones** under 5 cm are common.	Alternation of siltstones and mudstones with sandy beds indicate suspension interrupted by tractive currents (cf. Dalrymple *et al.* 2012). Soft-sediment deformation, indicating high-gradient slopes, and dropstones suggest **ice rafting**.
3	Sg-Flg (Fig. 4c)	Sandy siltstones with outsized clasts, fining-upward graded bedding and sharp-bounded. **Dropstones** are common. **Soft-sediment deformation** between poorly or non-laminated/stratified intervals occur. Locally these beds are fossiliferous and bioturbated. Layers are 10–30 cm thick.	Density flows, hemipelagic fallout and deformation due to slumping of beds during deposition. This facies could represent hyperpycnal flows, where the finer-grained outwash sediment carried in a buoyant meltwater plume rises suddenly to the free water surface and transports abundant fine sand, silt and mud (Mulder *et al.* 2003). Dropstones suggest **ice rafting influence**.
4	Tabular Sm (Fig. 4d)	Well-sorted, fine, tabular, massive, greenish-yellow sandstones showing diffuse borders. Horizons are 2–10 cm thick. Abundant tool marks (groove, bounce and prod casts). Bioturbation is present, as well as occasional small-scale load structures.	Rapid deceleration of a hyperconcentrated flow. Overloading and high sedimentation rates indicated by load structures. This facies implies high rates of sand supply in varying water depths from offshore to shoreface (cf. Clifton 2007; Johnson *et al.* 2002).
5	Dmm + Gm (Fig. 4e)	Lenticular beds of extraformational coarse diamictites and thin conglomerates (<0.20 m), usually amalgamated. Beds are 4 m thick. Lateral extension is no greater than tens of metres. Synsedimentary intraformational folds are common. **Faceted, bullet and striated clasts** are present (Dmax 10 cm).	Cohesive and fluid flows (hyperconcentrated and residual deposits, cf. Powell 1990; Mutti 1992), indicating **reworking of glacial deposits**. Synsedimentary-deformed glacial deposits characteristic of submarine gravitational resedimentation of subglacial till (cf. Eyles *et al.* 1985; Lønne 1995)
6	Dmm (Fig. 4f)	Tabular, massive and extraformational diamictites (granitic, metamorphic and limestones clasts). Beds are 0.50–3 m thick. Their lateral extension ranges from tens to hundreds of metres. Muddy to sandy matrix. Mx/Cl ratio is 10:1 to 1:1. Sub-rounded to rounded, **striated, faceted and bullet-shape clasts** are common (Dmax 20 cm).	Geometry and internal bed organization indicate density flows. Striated, faceted and bullet-shape clasts suggest **reworking of glacial deposits**
7	Dms (Fig. 4g)	Tabular, stratified diamictites with yellowish coarse sandy matrix. Beds are 10–50 cm thick separated by thin mudstone partitions. Bed lateral extension of tens of metres. Mx/Cl 5:1. Sub-rounded to rounded, **striated, faceted and bullet-shape clasts** (Dmax 8 cm) as well as outsized clasts rupturing strata (>40 cm) are frequent. More than 20% of the diamictites show stratification (similar to Dmm), represented by stringers and channels of gravels or intercalations of sandy/silty layers.	Stratification of diamictites indicate dilute subaqueous density flows. This process allows the differentiation of discrete layers of finely laminated tabular diamictites with thin mudstone partitions, suggesting settling product after episodes of drop mass and fluctuations in deposition from a meltwater plume (cf. Kellerhals and Matter 2003). Striated, faceted and bullet-shape clasts suggest **reworking of glacial deposits**. Outsized clasts are interpreted as **ice rafted debris**.
8	GGm (Fig. 4h)	Coarse, lenticular, poorly sorted, normally graded, cross-bedded conglomerates with very erosive base and boulders >50 cm in size. Greenish, brown or purple colour. Mx/Cl ratio 1:1. **Faceted, bullet and striated clasts** are observed. Clast composition: granites, metamorphic rocks, limestones, dark sandstones, felsic volcanic clasts.	Geometry and internal bed organization indicate turbulent high-energy diluted and turbulent flows. The colour variation of these channels suggests changes in oxidation conditions (subaqueous to subaerial). Striated, faceted and bullet- shape clasts are interpreted as **reworking of glacial deposits**
9	Shp (Fig. 5a)	Yellow-greenish and tabular sandstones with hummocky structures. Flat bases and ripples are common (climbing, wave and asymmetric).	Aggradation of sand originated by a combination of oscillatory and combined flow.
10	Smb + St (Fig. 5b)	Coquinite, detrital limestone consisting of shells or shell fragments, matrix to occasionally shell supported. Almost 95% brachiopods, rare nautiloids and bivalves. Fine sandstones with cross-stratification and occasional ripple lamination are interbedded.	Bioclastic bars, deposited in subtidal conditions (cf. Longhitano 2011).
11	Smq (Fig. 5c)	Poorly sorted, massive and coarse quartzitic sandstones (95% Qz, Dmax 1 cm). Tabular beds, normally amalgamated in sets >3 m, that show high angle cross-stratification and rare asymmetrical ripples.	Channels and bars of intertidal to subtidal sands.
12	Fine Sl + Sr (Fig. 5d)	Tabular, medium to fine, normally graded sandstones with low-angle to parallel stratification. Wavy structures are common. Normally 5–30 cm thick and 20–50 m lateral extension.	The normal grading and the parallel lamination suggest deposition from suspension and/or deposition as bedload transport by traction currents for the coarse-grained sandstones. The wavy structures may be an alternative sign of tractive currents and mud suspension under wave action.
13	Coarse Sp + St (Fig. 5e)	Coarse to medium sandstones, with large planar and/or trough cross-bedding structures. Beds >2 m thick. Normal gradation and usually amalgamated banks. Gravel layers and pelitic intraclasts are frequent.	Waning flows from tractional, high energy, fluid flows that reduces upward to low-flow regimes to decantation. Coarse gravelly sand on a high-energy coast.

(continued)

Table 1. *(Continued)*

	Facies	Description	Interpretation of processes
14	Sm (Fig. 5e)	Fine to very fine massive sandstones. Tabular (1 m thick), usually amalgamated without fine partitions. Occasionally, parallel diffuse lamination (1–5 cm), with asymmetrical ripples at the top. Many wisps of scattered lycophytes.	Clean sand, tabular geometry and massive arrangement suggests high-energy gravity flows. Ripples indicate wave action. Lycophytes could indicate foreshore to upper shoreface environments.
15	Gm (Fig. 5f and g)	Clast-supported and tabular conglomerates. Orange to yellowish sandy matrix. Poorly sorted. Slightly irregular base. Dmax 15 cm. Qz 70%, granites 15%, sandstone 10%, bioclasts 5%. Occasionally, 95% Qtz and very well rounded.	Turbulent high-energy traction currents. Unidirectional flows in shallow-water to subaerial settings. Locally, the compositional sorting and very well-rounded clasts suggest wave action.
16	Fine Dm (Fig. 5h)	Tabular, amalgamated diamictites (10–80 cm thick). Inverse gradation, from Mx support in the base (Mx/Cl ratio 10:1) to clast-supported (plug) at the top. Angular clasts Dmax 10 cm. Fangolitic Mx. Brown or purple colour.	Debris flows, shallow water to subaerial (cf. Postma 1990).

An abrupt upward transition from coarse-grained to finer lithologies represents the basal boundary of Sequence 4 (S4, from 95 to 110 m thick). Glaciomarine features, such as mudstones and fine sandstone with dropstones, are present at the base of S4. Profuse synsedimentary deformation is also common (FA C). The basal surface is interpreted as an erosional ravinement surface (cf. Clifton 2007) or a transgressive surface of erosion (TSE, cf. Catuneanu *et al.* 2009). Diamictites and conglomerate lenses, with numerous striated and faceted clasts, carve the muddy succession (FA D), suggesting the formation of subtidal channels where glacigenic sediments were transported over long distances. A shallowing-upward progradation is indicated by a progressive passage from inner shelf (FA C) to shoreface deposits (FA E, F and G). This succession is a stacked progradational sequence, where lower hierarchy sequences are separated by minor erosional surfaces formed during episodic flooding events (stacked parasequences from 570 to 610 m, see Supplementary Materials 1).

Sequence 5 (S5, from 40 to 115 m thick) starts with an upward transition from coarse-grained to finer lithologies interpreted as the beginning of the TST. The base of S5 is dominated by shally facies with dropstones and synsedimentary deformation that suggest ice rafting and iceberg grounding. However, we cannot rule out that this deformation is the result of mass transport (slumping and sliding) in lower shoreface to inner shelf environments (FA E and C). A thin pelitic interval without dropstones indicates an MFZ without glacial influence before the development of the next systems tract. This MFZ contains a diverse fossiliferous association (Fig. 3 and Supplementary Materials 1). The increase of typical lower shoreface, thick sandstone beds with dropstones and synsedimentary deformation towards the top (FA E) indicates an HST under glacial conditions that would represent an episodic glacial advance. The difference in thickness of this sequence between the studied localities (sections A and B, see Supplementary Materials 1) may be due to differential erosion of the regional erosive surface of the subsequent sequence (S6).

Sequence 6 (S6, *c.* 70 m thick) starts with a regional (km-scale) erosive surface developed between the top of S5 (deep-subtidal storm-bedded facies, FA E) and the bottom of S6. It is represented by amalgamated conglomerates and diamictites with numerous striated and faceted clasts that suggest density flows in ice-proximal glaciomarine to ice-contact proglacial environments. This surface is interpreted as a forced regression surface covered by proglacial subaqueous fan-deltaic facies that pass laterally into subtidal channels in deeper environments (FA A and B). This LST is followed by a fining-upward trend dominated by shally facies with progressively thinner-bedded and finer-grained sandstones (FA E and C), evidence of the development of the TST. The presence of sporadic channels, filled with amalgamated conglomerates and diamictites, is interpreted as delta-front slides and slumps, reworking glacial deposits derived from an onshore or tidewater

ice front in deep waters (FA D). The HST at the top of S6 is represented by lower to upper shoreface deposits (FA E, F and G). This is the uppermost sequence with unequivocal glacial evidence. Spores of middle to late Tournaisian age were described by Prestianni *et al.* (2015) in the HST of this sequence (Fig. 3 and Supplementary Materials 1).

Sequences 7 to 13 (S7 to S13, from 25 to *c.* 120 m thick, see details in Supplementary Materials 1) are formed of progradational systems with no glacial records and successive TST–HST. Facies are mainly characterized by offshore (FA C) to shoreface/deltaic facies (FA E, F, G and H), indicating a shallowing-upward trend (also coarsening-upward). Stacked sets of shoreline successions consist of progradational sequences separated by erosional surfaces formed during intervening transgressions (TSE). The subsequent highstand normal regressive shorelines typically show a progressive reduction in accommodation rates following the maximum flooding at the end of transgression. The topsets show a progressive increase in conglomerate and diamictite facies interpreted as shallow subaerial fan deltas to shoreface environments. The thickening and coarsening-upward trend with cross-bedding structures along the shoreface successions suggest an upward increase in depositional energy. Normal regressions are typically accompanied by increasing aggradation, with progradation rates being inversely proportional to the rates of topset aggradation (e.g. Catuneanu *et al.* 2009). The topset aggradation rates would be related to the rates of relative increase in coastal elevation. Progradation rates therefore tend to increase with time during highstand normal regressions (cf. Catuneanu and Zecchin 2013). This trend is reflected in the thickness of the beds composing the topset units.

Sequence 14 (S14, *c.* 140 m thick) represents a coarsening-upward succession and the beginning of the deposition of the Cerro Tres Cóndores Formation. S14 developed over a subaerial unconformity interpreted as a BSFR. Basal deposits are dominated by lenticular and coarse conglomerates interbedded with coarse diamictites and occasional greenish lithic sandstones (FA H). The gravelly beds show rounded clasts but sorting is very poor. The maximum clast size is 0.25 m, suggesting a substantial increase with respect to the granulometry of previous successions. The presence of coarse sandstones with cross-stratification interbedded with imbricated coarse, poorly sorted conglomerates is a common association of shelf-margin fan deltas (Lønne 1995). The presence of occasionally striated and faceted clasts suggests that these conglomeratic systems could have developed as lateral proglacial environments, probably associated with glacial retractions or the result of reworked glacial deposits. The existence of subaerial and subaqueous deposits indicates a regressive trend after the generation of the BSFR, associated with a major base-level fall (falling-stage systems tract, FSST, cf. Catuneanu 2017). The progressive decrease in the coarse fan-deltaic channel facies in relation to the psamitic shoreface facies (FA G) is interpreted as a

Table 2. *Description and interpretations of facies associations (FA) of the Agua de Lucho and Cerro Tres Cóndores formations in southern Sierra de Las Minitas. Bold letters indicate the most abundant and diagnostic facies*

FA	Facies	Description	Interpretation	Depositional environment
A	**Dmm** **Ds** **Dms** **Gm** **Sm** **Fl(d)**	This association is dominated by greenish-grey or maroon diamictites and coarse conglomerates that represents >80% of the facies association (Dmm, Ds, Dms, Gm). Bedding is poorly developed and can usually only be seen where diamictites are interbedded with conglomeratic and sandy wedges (Sm). Locally, Fl interbeds and are occasionally deformed (Fig. 4e). Striations are common on the fine-grained clasts. Faceted clasts are common.	Subaqueous deposition from: (a) rainout from a high concentration of debris-rich icebergs; or (b) from sediment-laden efflux jets close to the grounding line of a glacier or ice sheet. Conglomerate facies represent erosional lags or mass flow deposits. The Fl (d) facies are interpreted as occasional suspension settling subsequently deformed after episodes of drop mass.	**Subaqueous channels in a fan delta.** Ice contact proglacial settings with rework of glacial deposits.
B	**Sm** **Smq** **Dm** **Ds** **Gm** **Gs**	Pale yellow to greenish-grey, moderately to well-sorted sandstones (Sm, Smq) are commonly interbedded with the diamictites (Dm, Ds) and conglomerates (Gm, Gs) and form laterally continuous sheets or discontinuous lenses. Bed thickness varies widely, from 0.2 cm to 3 m. This association shows a thinning- and fining-upward trend is common, as is an erosive base. Outsized clast (dropstones) are common in sandstones and diamictites. Multi-storey bodies interfinger with the surrounding turbidite facies associations (FA C, see below).	The interfingering of multi-storey channel deposits with rain-out diamictites and turbidites with dropstones indicate a subaquatic glaciomarine depositional environment. Tabular sandstones are interpreted as deposition and subaqueous outwash fan deposits. This facies association suggests a proximal subaqueous deposition through the release of debris from subglacial conduits at the grounding-line fan, locally with subsequent wave rework.	**Shoreface proximal to ice front. Local ice rafting.**
C	**Fl** **Fl + Sr** **Sg-Flg** Dmm + Gm	Mudstone beds (Fl), rhythmites (Fl + Sr) and density-flow deposits (Sg-Flg) with outsized clasts (dropstones) and occasional interbedding deformation (recumbent folds) under massive diamictites and conglomerates (Dmm + Gm) with intraclasts and lenses of the underlying rhythmite. Intense bioturbation.	Turbidites deposited in flat shallow channels by numerous pulses of turbiditic events. During the pauses between consecutive turbidites, deposition of sediment from rain-out of icebergs is suggested by intercalations of Dmm and dropstones. Deformation would be associated to overlying mass transport.	**Inner-outer shelf. Local ice rafting.** Quiescent subaqueous sedimentation during an ice retreat phase.
D	**Dmm + Gm** **Fl + Sr** **Smq**	Amalgamated tabular to lenticular conglomerates and diamictites (Dmm + Gm) directly overlie through large-scale erosive contact on top of fine deposits (Fl + Sr). Concave-upward medium-scale erosive bases and planar tops. Lateral continuity >500 m. Individual bodies show fining-upward arrangement with sandstones at the top (Smq). Mud drapes.	Migration of 2–3D dunes during high-energy conditions related to unidirectional tractive currents. The erosive bases, the lenticular geometry and the fining-upward arrangement suggest that these conglomerates were deposited as the infill of channels. The mud drapes, attributed to recurring energy variations that allow suspension settling of fine-grained material, together with the outcrop geometry, indicate tidal currents.	**Subtidal channels**
E	**Sm/Sg-Flg** Fl + Sr	Sandstone-dominated packages with a lower mud proportion in comparison with FA C. Sm and Sg-Flg alternating with Fl + Sr (3:1 to 10:1). Dropstones are present. Intense bioturbation.	They represent ripple migration processes and settling from suspension during fair-weather conditions, alternating with sand accumulated by oscillatory and combined flows during storm events. Dropstones suggest ice rafting influence.	**Lower shoreface.**
F	**Shp** **Smq** **Fine Sl + Sr** Fl + Sr Smb	Sandstones with hummocky and ripple structures (Shp), alternating with coarse, massive and normally amalgamated sandstones (Smq). Tabular sandstones with low angle parallel stratification and wavy structures (Sl + St). Interbedded layers of silt and mud (<10%). Occasional coquinites. Moderate bioturbation.	This FA is interpreted as the result of 3D subaqueous dune migration during high-energy conditions dominated by wave action. The coarse to medium sandstones and the interbedded layers of silt and mudstones reflect deposition between fair-weather wave base and storm wave base. Sr intercalated with mudstones suggests moderate-to-low energy conditions. Coquinites are interpreted as bioclastic bars, deposited in subtidal conditions. Lithofacial changeability is interpreted as alternating storm and fair-weather conditions typical for shallow marine strata.	**Middle shoreface.**
G	**Coarse Sp + St** **Fine Sl + St** **Sm** **Gm**	Tabular and coarse Sp + St delimited by irregular bases and undulated tops, and displaying a coarsening and thickening-upward arrangement. Alternation of Sm and fine Sl + St (<20%). Gm are common.	The sedimentary structures, texture and the general arrangement of the sandstones suggest deposition in high-energy settings, well above fair-weather wave base.	**Upper shoreface**
H	**Gm** **GGm** **Dm** **Sm** **Sl + St**	The coarse conglomerates are lenticular beds showing broad stratification and cross-stratification. Gradual decrease in grain size from poorly sorted coarse-grained conglomerates and fine diamictites through wave imbricated fine-grained conglomerates and tabular cross-bedded and planar laminated sand.	The transport mechanism was a traction current derived from a unidirectional and constant source. Conglomerates have a possible fluvial origin, with subsequent wave rework.	**Shallow water/shelf type fan-delta**

transition to an LST. Thin intervals of wave-rippled sandstones intercalated with mudstones (FA F) suggest moderate to low energy conditions in a middle shoreface, and are interpreted as the

MFZ. This TST developed in response to periods of decreasing low-clastic input to the shoreline or increasing accommodation. The overlying regressive HST records a renewed, increasingly
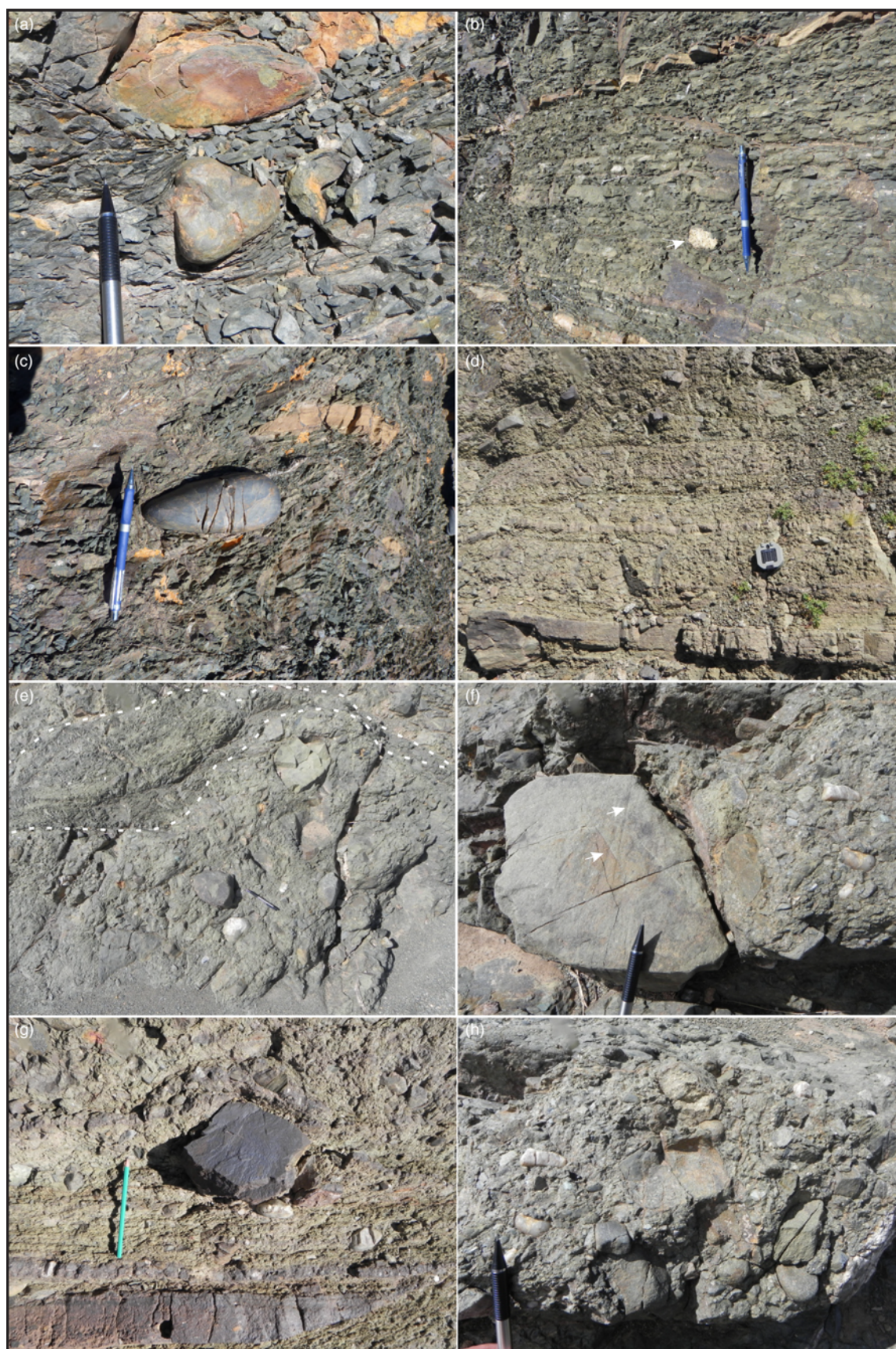
Fig. 4. Photographs representative of lithofacies listed in Table 1. See Supplementary Materials 1 for location of the photographs in the stratigraphic sections. (**a**) Facies 1, laminated mudstones with dispersed gravel and an impact depression beneath the outsized clast, indicating that the mud has been deformed beneath ice-rafted dropstones. (**b**) Facies 2, interbedded mudstones and fine-grained sandstones, with dispersed extraformational gravel of granite composition (arrow). (**c**) Facies 3, sandy siltstone with dispersed gravel. (**d**) Facies 4 and 7, massive, well-sorted sandy beds interbedded with stratified diamictites with outsized clasts. (**e**) Facies 5, cohesive debris-flow lenses (diamictitic, with outsized clasts) intercalated with synsedimentary-folded sandy wedge. (**f**) Facies 6, faceted and striated clast observed in tabular diamictite. White arrows indicate some of these striations. (**g**) Facies 7, stratified thin diamictites with outsized clasts. (**h**) Facies 8, lenticular, massive, polymictic and poorly sorted bed in the clast-supported conglomerate.

Fig. 5. Photographs representative of lithofacies listed in Table 1. See Supplementary Materials 1 for location of the photographs in the stratigraphic sections. (**a**) Facies 9, tabular sandstones with hummocky cross-stratification. (**b**) Facies 10 is a coquinite, a limestone formed almost entirely of sorted and cemented fossil debris, most commonly coarse brachiopod shells and shell fragments. (**c**) Facies 11, a coarse-grained quartz sandstone with high-angle cross-stratification. (**d**) Facies 12, medium to fine sandstones with low-angle to parallel stratification and often wavy-bedded structures. (**e**) Facies 13 (F13), lenses of coarse and yellowish sandstone, with trough cross-bedding structures; and facies 14 (F14), tabular and amalgamated, fine to very fine massive sandstones. Both facies are interpreted as high-energy flows in foreshore to upper shoreface environments. (**f**) Facies 15, >30 m of a continuous succession of irregular lenses of coarse to fine quartz conglomerates. (**g**) Facies 15, details of clast-supported, poorly sorted, well-rounded and quartzitic conglomerates. Normally these are massive lenticular beds with markedly erosive bases. (**h**) Facies 16, tabular diamictites, with inverse gradation, from Mx-supported in the base to clast-supported (plug) at the top. Note the angular clasts. Mx of fangolites.
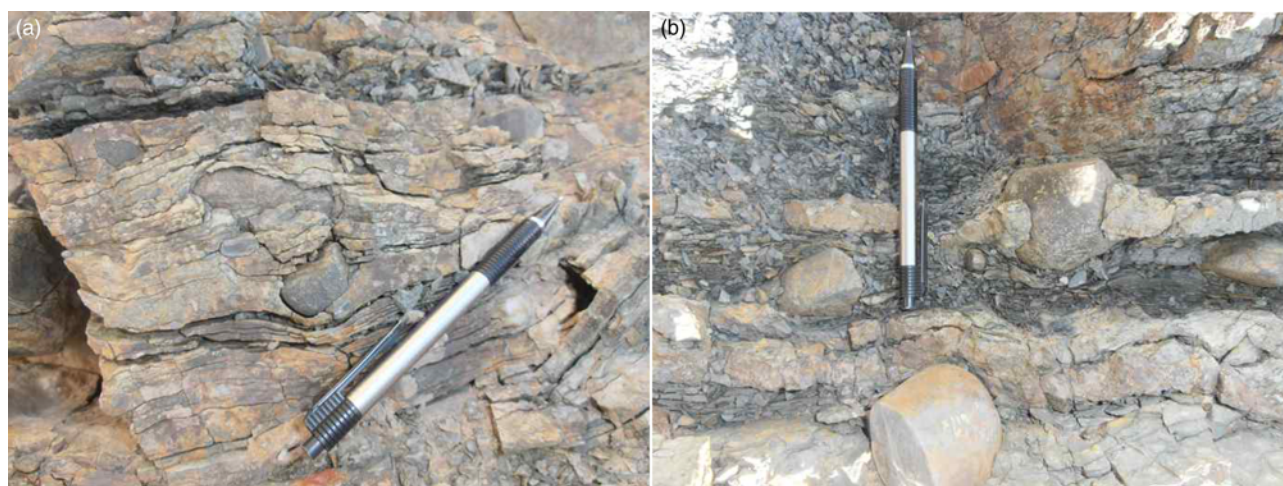
Fig. 6. (a) and **(b)** Dropstones in heterolithic facies. Note basal lamination folding, drape structure of the laminated sediments over the clasts and the characteristic morphology of bullet-nose facet of pebble.

high-clastic input (FA H) or decreasing accommodation, resulting in fan delta progradation.

S15 is poorly preserved and could only be reconstructed in the eastern section B of Agua Quemada syncline (Fig. 1 and Supplementary Materials 1). It is partially covered and its base is not exposed. The studied sections contain a TST followed by a regressive HST, similar to the S14 arrangement. The detrital zircon sample (MIN-190, see below) was taken in the HST interval.

Provenance analysis of the Cerro Tres Cóndores Formation

Conglomerate composition and palaeocurrents

On the Cerro Tres Cóndores hill (Fig. 1), this formation is dominated by lenticular, coarse lithic sandstone (>50% lithic fragments) and conglomerates, with clast composition dominated by coarse subarkosic sandstones and dark grey greywackes to meta-greywackes (*c.* 72%), granites (*c.* 15%), green shales (*c.* 8%) and volcanics (*c.* 5%). In these outcrops, scarce palaeocurrent data (n = 8) show a SW flow direction (mean vector = 233°) with little dispersion. On the Punta Negra hill (*c.* 5 km E of the stratotype, Fig. 1), clast composition is dark sandstones (*c.* 57%), felsic volcanics and granites (*c.* 25%), gabbros and pillow basalts (*c.* 12%) and marble and phyllites (*c.* 6%). The predominant SSE palaeocurrents (mean vector 171°, n = 34) show high dispersion of data (see Supplementary Materials 2) consistent with braided channels in fan systems.

On Mudadero hill (*c.* 10 km S of the stratotype, Fig. 1), the Agua de Lucho Formation (upsection) shows a progressive and concordant passage to the coarser successions of the Cerro Tres Cóndores Formation, which consists mainly of a sandy succession with scarce, interspersed conglomeratic facies. These conglomeratic lenses record abundant pelitic clasts (*c.* 87%) recycled from the lower unit. Palaeocurrents show an average SW direction (226° mean vector, n = 18).

In the southern part of Sierras de Las Minitas (*c.* 25 km SW of the stratotype), the conglomerate clasts are represented by quartz-rich fragments (*c.* 53%), granites (*c.* 25%) and metamorphic rocks (*c.* 9%). It is important to highlight that in numerous conglomeratic beds, the compositional distribution corresponds to quartz clasts (*c.* 80%), granites (*c.* 10%), volcanics (*c.* 5%) and metamorphic rocks (*c.* 5%). The matrix content is quartzose sandstone/quartzite. Palaeocurrent data indicate multiple flow directions towards the SW and W (248° mean vector, n = 22).

U–Pb detrital zircon data from the Cerro Tres Cóndores Formation

The sample (MIN-190) is a quartzite-clast and quartzose matrix conglomerate collected at the uppermost outcrop of the Cerro Tres Cóndores Formation at section B (S15, *c.* 200 m above the bottom of this unit, see Supplementary Materials 1). A total of 76 zircon grains were dated, and further information on values and methodology, together with photographs, can be found in Supplementary Material 3. The analysed zircons have the following variable morphologies, recognized in decreasing abundance (Fig. 7a): (i) euhedral and subhedral prismatic; (ii) fragmented prismatic; and (iii) rounded grains. The zircons mainly display oscillatory zoning.

The Concordia diagrams indicate that most of the analysed zircons plot on the Concordia line, bracketing the interval 358–1865 Ma (Fig. 7a–c). The detrital zircon distribution pattern (Fig. 7d) shows a small group of Neoproterozoic ages, with Ediacaran (n = 2) and Cryogenian (n = 2) ages, respectively. The large Mesoproterozoic spectrum shows a peak at 1030 Ma (n = 7) and two subordinate peaks at 1232 (n = 5) and 1375 Ma (n = 5). The largest group is made up of early Ordovician (Tremadocian) ages with a peak at 480 Ma (n = 22). Three grains define an early Silurian subordinate peak (427 Ma), while two grains at 1847 and 1893 Ma (Palaeoproterozoic) define the complete population (Fig. 7a–d). The youngest zircon age is 358 Ma (Fig. 7a–d), which represents the Devonian–Carboniferous boundary (358.9 ± 0.4 Ma, Ogg *et al.* 2016). Although this age was obtained from a single zircon grain, it is strongly consistent with palaeontological data.

Discussion

Provenance analysis and basin implications of the detrital zircon age data

Provenance analysis suggests that the main source of the Cerro Tres Cóndores Formation was mainly the Sierras Pampeanas and locally northern Precordillera basements, located to the east and north of the study area. The composition of the clasts in different conglomeratic facies shows a high proportion of Lower–Middle Paleozoic rocks exposed near the study region (e.g. Collo *et al.* 2008).

The detrital zircon age spectra of the bottom section of the Cerro Tres Cóndores Formation (Fig. 7d) suggests a clear input from the Proterozoic to Lower Paleozoic basement of the Sierras Pampeanas, mostly exposed to the east. Mesoproterozoic and Neoproterozoic ages are recognized in the 'Pampean' basement exposed in the Sierras de Córdoba, Sierra Brava and Sierra de Ancasti (Rapela
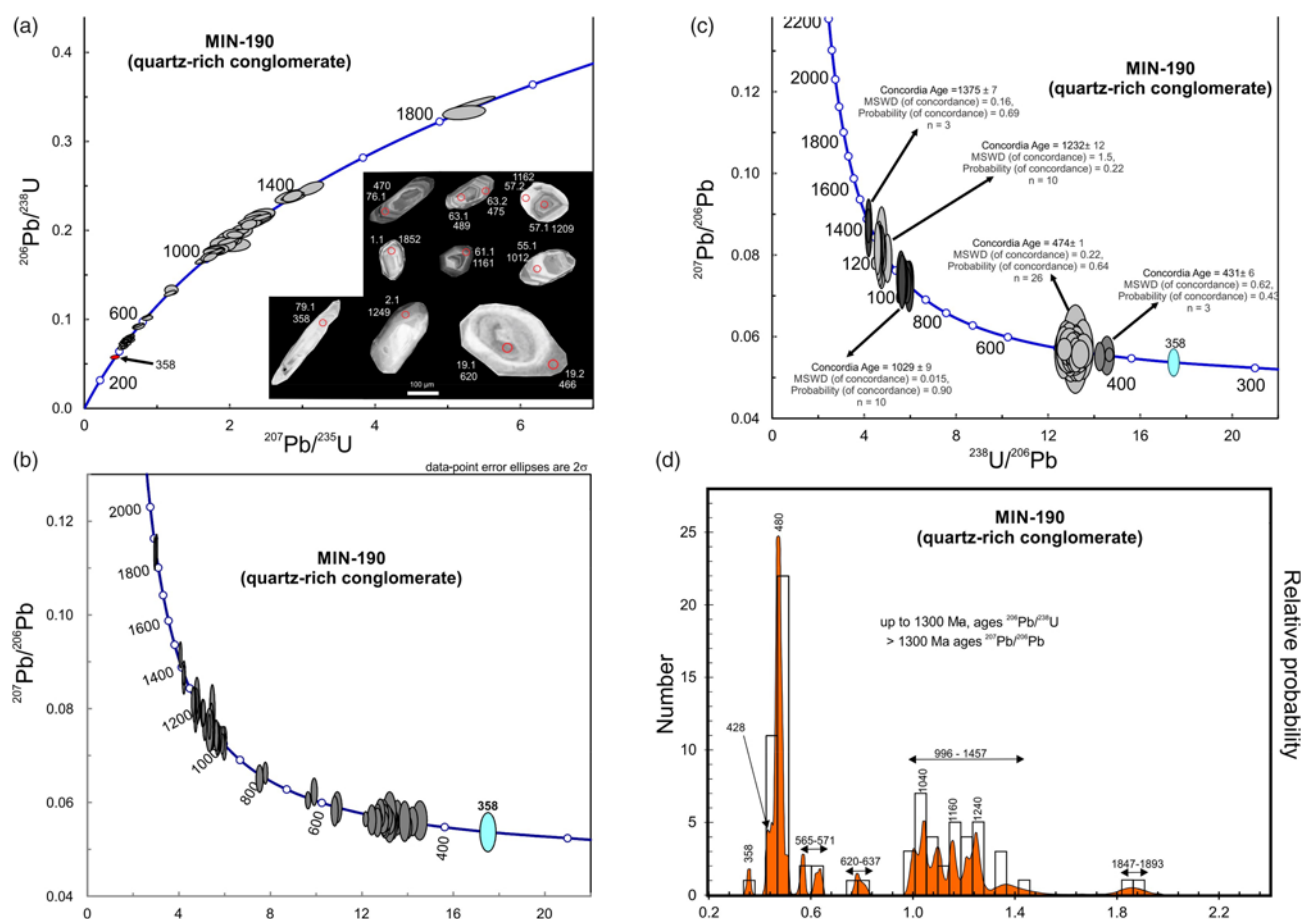
Fig. 7. (a) Wetherill-type and **(b)** Tera–Wasserburg plots for detrital zircon U–Pb LA-MC-ICP-MS data of the Cerro Tres Cóndores Formation, sample MIN-190. Analyses with an error greater than 10% were rejected. The youngest zircon age is in red colour. **(c)** Tera–Wasserburg plots and calculated ages for detrital zircon U–Pb LA-MC-ICP-MS data of the Cerro Tres Cóndores Formation, sample MIN-190. n = number of analyses used in the calculation (data in Supplementary Materials 3). **(d)** Zircon probability density plots from Cerro Tres Cóndores Formation, sample MIN-190. Representative zircon morphology is shown in (a), where number of spot (e.g. 57.1) and ages in Ma (e.g. 477) are reported. All the analysed zircon grains are displayed in Supplementary Material 3.

et al. 2016, 2007). Nevertheless, Mesoproterozoic ages ranging from *c*. 1.0 to 1.4 Ga similar to those reported in Figure 7d were recognized in the western Sierras Pampeanas (Sierra de Maz, see Rapela *et al.* 2016 and references therein), to the SE of the study region. Similar Mesoproterozoic age ranges, together with Neoproterozoic ages (peak in 620 Ma), as shown in Figure 7d, were reported in the southeastern basement of the Sierra de Pie de Palo (SE of the Sierra de Las Minitas), known as Difunta Correa Metasedimentary Sequence (Rapela *et al.* 2016). The age peak at 480 Ma is typical of the Ordovician igneous rocks exposed at Sierras Pampeanas and the Famatina area, supporting an eastward provenance (e.g. Dahlquist *et al.* 2013 and references therein). Ages around 430 Ma have also been recognized in the Sierras Pampeanas (e.g. Casquet *et al.* 2005).

It is important to note the lack of zircon ages in the ranges of 2.02–2.26 Ga (Río de La Plata Craton, Rapela *et al.* 2007), 540–515 Ma (Pampean magmatism, Iannizzotto *et al.* 2013; Von Gosen *et al.* 2014 and references therein) and 379–366 Ma (middle–late Devonian batholiths of the eastern Sierras Pampeanas such as the Achala batholith, Dahlquist *et al.* 2013). It is also important to highlight the absence of late Tournaisian–Visean zircon ages representative of local igneous rocks. This includes the range from 348–342 Ma (rhyolitic successions of the Cazadero Grande Formation exposed <100 km to the NE, Martina *et al.* 2011; Coira *et al.* 2016), the nearby Potrerillo pluton (353 Ma, see location in Fig. 1) and the Veladero and Río Bonete stocks, with ages of 347 and 342 Ma, respectively (Dahlquist *et al.* 2018a,b).

Most of these ages are probable sources exposed in pericratonic areas in the easternmost Sierras Pampeanas, suggesting distance control or, in the case of the potential lower Carboniferous source, no exhumation or detrital damming.

Detrital zircon ages of the Cerro Tres Cóndores Formation are roughly similar to those reported for the overlain Punta del Agua Formation (Báez *et al.* 2014) and the Huasco metamorphic complex (Álvarez *et al.* 2011). The most significant difference is that these units show ages of 337 Ma and 342 Ma respectively, indicating a Visean maximum depositional age for these formations. Recently, Dahlquist *et al.* (2018a) described ages from metasedimentary and igneous rocks from the Cerro Veladero area (40 km to the south of Sierra de Las Minitas), reporting detrital zircon age patterns ranging from 342 ± 2 to 347 ± 4 Ma. This age range is similar to the volcaniclastic Cazadero Grande Formation (342–348 Ma, Coira *et al.* 2016), located 100 km to the north. In turn, Gallastegui Suárez *et al.* (2014) reported an age of 348 ± 2 Ma for a granitic clast (retro-arc A-type granitic rocks, cf. Dahlquist *et al.* 2013) included in the lower Carboniferous Del Ratón Formation in the Precordillera of Argentina, 150 km to the SW of the study region. This igneous clast might have originated from the Sierras Pampeanas, or from small Carboniferous bodies exposed in the Cordillera to the SW of the study area.

The early Carboniferous ages absent from the Cerro Tres Cóndores Formation therefore suggest that this unit is older than the Visean volcanism of the Punta del Agua and Cazadero Grande formations, and also precedes the Del Ratón and the Huasco formations. Notably, detrital zircon age patterns from the Punta del

Agua Formation (Báez *et al.* 2014) are very similar to those reported for MIN-190, leading us to hypothesize that the source area was continuous during the deposit of the Agua de Lucho, Cerro Tres Cóndores and Punta del Agua formations.

In synthesis, the composition of clast conglomerates, together with palaeocurrent measurements and detrital zircon age spectra, suggest a source area in the Sierras Pampeanas basement indicating relief formation and sediment supply from the east. Limarino and Spalletti (2006) defined for this region the presence of an important orogenic relief, known as the Proto-Precordillera, whose uplifting would have occurred between the Late Devonian and Mississippian. However, the provenance analysis on the Cerro Tres Cóndores Formation suggests that this topographic high would not have been a relevant source by this time. On the contrary, it would have constituted a bypass zone for sediments coming from the east. This is contrary to the hypothesis that the Agua de Lucho and Cerro Tres Cóndores formations represent synorogenic deposits sourced from the Proto-Precordillera (Limarino *et al.* 2017).

What driving mechanisms controlled the evolution of the Mississippian sequence?

The palaeontological and geochronological data analysed herein indicate that the *c.* 1400 m-thick studied section was deposited between the middle to late Tournaisian (*c.* 5 My). The 15 stratigraphic sequences described above can be grouped into three sequential models (Fig. 8):

(1) *Non-glacial TST–HST sequences*. This model is represented by S7 to S13 (Fig. 8a and Supplementary Material 1). The vertical arrangement starts with fine deposits at the base, overlying a flooding surface, which are the product of rapid subsidence and consequent transgression (TST). These relatively deep-water deposits characterize the underfilled phase in the evolution of the basin. Then the succession begins to prograde basinward, developing upwards to shallow-water and coastal systems (filled phase), which could grade to fluvial facies atop (overfilled phase) (HST). The general change from underfilled to overfilled conditions is attributed to a shift in the balance between the processes that generate basin accommodation and the ability of sedimentary systems to fill the available space. The TST includes retrogradational facies that accumulated during a tectonically driven pulse of subsidence and flooding. The HST forms the bulk of the sequence, and includes the progradational coarsening-upward succession that overlies the maximum flooding surface. Due to the asymmetrical shape of the base-level (accommodation) curve, with fast rise (pulse of tectonic subsidence) followed by prolonged stillstand (tectonic quiescence), the LST tends to be poorly developed or absent. This marks a significant difference between extensional settings and tectonically stable basins such as those represented by continental shelves in passive margin settings (Martins-Neto and Catuneanu 2010). However, the absence of indicators of local ice does not necessarily mean than a relative sea-level change, unconnected of glacial processes; could be related to initiation and growth of ice sheets remotely. Thus, it cannot be ruled out that glacio-eustasy could have played a complementary role in the generation of accommodation space (cf. Zecchin *et al.* 2010).

The tectonically controlled stratigraphic framework of depositional sequences in extensional settings, bounded by flooding surfaces and arranged internally in several dominantly coarsening-upward successions, characterizes the architecture of sequences that develop at different hierarchical levels (Catuneanu *et al.* 2009; Dalrymple *et al.* 2012). Higher-frequency sequences (less than 10 m) can be recognized, where smaller-scale sequences display the same coarsening-upward character. Such higher-frequency sequences could be attributed to smaller-scale tectonic pulses of fault reactivation that occur between the major tectonic events, during a time of long-term tectonic quiescence. A renewed subsidence pulse leads to drowning the previous deposits and starts a new depositional sequence (Catuneanu *et al.* 2009; Martins-Neto and Catuneanu 2010). It cannot be ruled out that these higher-frequency sequences could be related to increases in sediment supplies associated with climatic variations. The lack of chrono-stratigraphic precision in these intervals goes against better definition.

(2) *Glacial-influenced sequences.* Variations from the typical TST–HST sequence can occur due to global and local factors. The overprint of climate-driven sea-level fluctuations is critical. In temperate glacial environments, the maximum glacial advance is reflected as forced regressions followed by an LST stage (Fielding 2018). This sequential model represents S2, S3 and S6 (Fig. 8b and Supplementary Material 1). These sequences start with a basal erosive boundary defined by an increase in coarse-grained and gravelly lithologies. These deposits could be interpreted as an LST associated with a glacial maximum. They are proximal to distal glacial diamictites, sometimes interbedded with conglomerates and sandstones. A fining-upward sequence, formed of sandy levels to muddy beds with dropstones, laps onto the previous tract. This could be interpreted as a TST associated with a glacial retreat during a progressive relative sea-level rise. Overlying this, bioturbated siltstones with marine invertebrate fossils are common. Generally, no oversized clasts are observed in this level, which is interpreted as a MFZ with no glacial indicators (ice minimum). A coarsening-upward trend is indicated by a transition to a sandstone-dominated interval with current and wave-generated sedimentary structures. During glacial retreat, the systems tracts prograde due to high sediment flux with deltaic sedimentation, exceeding the creation rates of accommodation spaces. This results in the formation of a HST. This section is truncated by the following sequence boundary.

In this model, each sequence represents relative sea-level changes associated with the advance-retreat events of glaciers, with the influence of ice activity. These sequences coincide with the idealized glacial sequence model proposed by Fielding (2018). It is important to note that this model explains the intermittent glacial records in an extensional basins context, in which sea-level fluctuations result from the combination of autocyclic, palaeo-climatic and tectonic activity. However, unlike Fielding (2018), our model includes lower fining-upward and upper coarsening-upward sets quite similar to that described for sequences that represent a progressive removal of ice and a consequent glacio-isostatic effect (Dietrich *et al.* 2018). This suggests that the sequences described here might be (at least partially) a consequence of a relative sea-level fall, related to the glacial-driven isostacy rather than a glacial-driven palaeo-eustatic fall associated with an ice sheet growth, or a highstand progradation during an interglacial episode. After an event of glacial unloading, the Earth deforms viscously on time scales of 10^3–10^5 yr as the mantle flows back into the depressed region (Conrad 2013). This triggers uplift in the region near the former ice sheet, causing (at least locally) a relative drop in sea-level (Farrell and Clark 1976; Clark and Primus 1987; Davis and Mitrovica, 1996). On time scales of 10^6 yr, and longer, sea-level changes are mainly controlled by plate tectonics and mantle dynamics (Harrison 1990; Miller *et al.* 2005).

In S1, S4 and S5 there are no records of a basal LST (see Supplementary Material 1). These TST–HST sequences contained dropstones and occasional thin conglomerates with striated clasts in a delta-front landslide, suggesting ice rafting and reworking of glacial deposits. This indicates an interaction of stages in which the accommodation space progressively diminished, with the sporadic
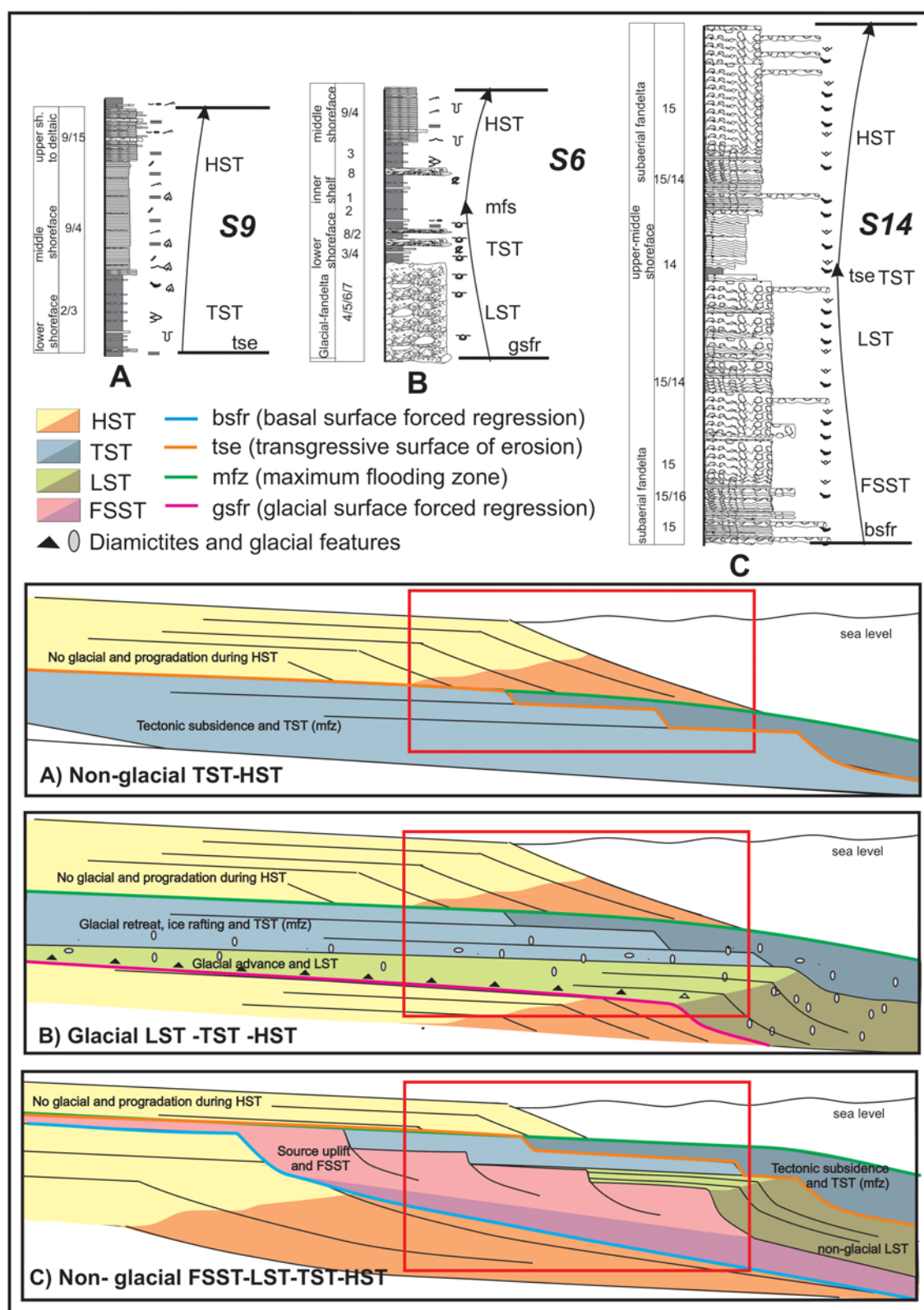
Fig. 8. Graphic logs summarizing the three sequential models and their location in a synoptic transect from on-shore to off-shore (red rectangle). (**a**) Graphic log of S9 showing a non-glacial TST–HST sequence model, with a basal transgressive surface of erosion (TSE) in which the accommodation space is mainly conditioned by tectonic subsidence. (**b**) S6 an example of the advance and retreat of glaciers. GSFR (glacial surface forced regression) represents the basal sequence boundary. Glacial Lowstand Systems Tract (LST) is formed of diamictites and conglomerates with glacial imprint. In the transgressive stage (TST), dropstones and soft-sediment deformation structures are characteristic of ice rafting. Maximum flooding zone (MFZ) usually has a high fossil content. The Highstand Systems Tract (HST) does not normally have glacial records. (**c**) Graphic log of S14 as a non-glacial FSST–TST–HST sequence model, which shows a marked basal surface forced regression (BSFR) interpreted as a relative sea-level fall associated with a source area uplift.
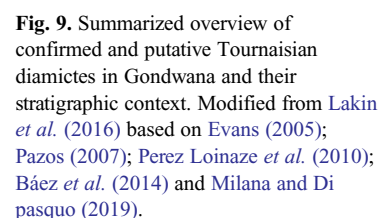
glacial record suggesting an ice-distal position. These shallow-marine transgressive–regressive cycles with the presence of glacial features could be linked to glacio-eustatic changes (cf. Zecchin *et al.* 2010).

(3) *Non-glacial forced regression sequence*. Another model of sequence stratigraphic architecture is defined by S14, which represents a relative sea-level fall associated with a forced

regression (falling stage systems tract, FSST, cf. Catuneanu 2017, Fig. 8c and Supplementary Material 1). It refers to a stratal stacking pattern defined as a downstepping of the shoreline. The absence of glacial evidence suggests that this fall in relative sea-level is not associated with a local glacial stage. In S14, forced regression accompanied by the formation of a basal subaerial unconformity imply that previous marine deposits were subject to erosion or sediment bypass. The normal regression that follows this forced regression is designated as a lowstand normal regression (LST) in response to the increase in accommodation rates followed by a relative sea-level rise (TST). The normal regression that follows the TST is designated as a highstand normal regression (HST), where the rates of accommodation decrease following the MFZ at the end of transgression.

The development of very proximal conglomerates with large boulders, as well as the provenance of the Cerro Tres Cóndores Formation (clast conglomerate composition, palaeocurrents and detrital zircon ages), suggest exhumation and relief formation to the east since *c.* 350 Ma. We disregard a local glacio-isostatic adjustment to explain this regional uplift, since this unit is deposited 500 m (and six sequences) above the last glacial record (see Supplementary Materials 1) and is not consistent with the response time of this post-glacial rebound, which has a duration on timescales of thousands to hundreds of thousands of years (cf. Milne and Mitrovica 2008; Dietrich *et al.* 2018). Glacial isostatic adjustment would have been over long before Sequence 14 was deposited (10^5 to 10^6 Ma later). It is important to remember that the next glacial event in this region occurred *c.* 12 myr later (Limarino *et al.* 2014; Milana and Di Pasquo 2019, Figure 9), thereby ruling out a glacio-

isostatic origin. However, an important drop in sea-level in northern Gondwana at the Tournaisian–Visean boundary is considered to record the development of an ice cap and to herald a change to the Carboniferous climate with glaciations (Lees 1997; Bábek *et al.* 2013; Poty 2016). Nevertheless, the lack of temporal accuracy of the FSST at the base of the Cerro Tres Cóndores Formation (late Tournaisian to early Visean) does not allow us to establish with exactitude this global sea-level fall as the main cause of the generation of this surface. On the other hand, according to the regional setting, an alternative is related to an isostatic rebound by crustal/lithospheric thinning, as suggested by palaeotopographic analysis and mafic rock geochemistry (cf. Martina *et al.* 2011; Dávila *et al.* 2017).

Glacial extent during the middle Tournaisian

It is widely acknowledged that the LPIA began at the end of the Famennian and lasted until the middle Permian (Isaacson *et al.* 2008; Caputo *et al.* 2008; McGhee 2018; Montañez and Poulsen 2013). However, little is known about the temporal and geographic extent of ice centres during most of the Mississippian (Caputo *et al.* 2008; Lakin *et al.* 2016). Although the Tournaisian has usually been regarded as an interval where cold climates prevailed (Rygel *et al.* 2008), there is ambiguous evidence for the presence of ice centres (Saltzman 2002; Frank *et al.* 2008; Lakin *et al.* 2016).

Ice-distal isotopic and stratigraphic data suggest the presence of ice centres in Gondwana. Tropical brachiopod calcite δ18O values indicate a short but important cooling event in the middle Tournaisian, with tropical sea temperature lower than the last glacial maximum (Giles 2012). Conodont apatite δ18O values also

Fig. 9. Summarized overview of confirmed and putative Tournaisian diamictes in Gondwana and their stratigraphic context. Modified from Lakin *et al.* (2016) based on Evans (2005); Pazos (2007); Perez Loinaze *et al.* (2010); Báez *et al.* (2014) and Milana and Di pasquo (2019).

point to a climatic cooling comparable to the transition to the last glacial maximum (Buggisch *et al.* 2008). Moreover, a short, global mid-Tournaisian δ13C excursion occurring at the same time also underscores glaciation across Gondwana (Saltzman 2003, 2002; Buggisch *et al.* 2008; Yao *et al.* 2015). The bulk of these data agree with stratigraphic information that suggests glacial eustasy close to the Kinderhookian–Osagean boundary (Matchen and Kammer 2006; Kammer and Matchen 2008; Wallace and Elrick 2014).

Although the Tournaisian regularly experienced intermediate eustatic changes (20–25 m), such fluctuations cannot be unquestionably regarded as evidence for glacial eustasy (Rygel *et al.* 2008). However, high-frequency stratigraphic cycles coupled to shifts in conodont apatite δ18O in the latest Kinderhookian do attest to sea-level changes of *c.* 40 m, which were most probably caused by the waxing and waning of glaciers (Wallace and Elrick 2014). In addition, an extensive unconformity at the Kinderhookian–Osagean boundary across North America, recording a *c.* 60 m sea-level drop, further supports the growth of ice centres in the Southern Hemisphere (Matchen and Kammer 2006; Kammer and Matchen 2008). These eustatic fluctuations suggest ice volumes ranging from *c.* $15*10^6$ km^3 to *c.* 28×10^6 km^3 and a minimum glaciated area of *c.* $6.5*10^6$ km^2 (following Crowley and Baum 1991; Isbell *et al.* 2003).

Such expected ice volume and glaciated areas based on records from North America contrast with the scarce record of mid-Tournaisian glacigenic sedimentary deposits in Gondwana (Caputo *et al.* 2008; Playford *et al.* 2012; Lakin *et al.* 2016). Positively identified mid-Tournaisian diamictites in South America are currently limited to the subsurface of northern Brazil (Caputo *et al.* 2008; Playford *et al.* 2012). Although both Caputo *et al.* (2008) and Playford *et al.* (2012) indicated that these diamictites extend throughout the Solimões, Amazon and Parnaíba basins (Fig. 9), Lakin *et al.* (2016) pointed out that only Parnaíba diamictites have been described and biostratigraphically constrained. Glacial records in the Valle Chico Formation from Tepuel Genoa Basin in Patagonia recently assigned to the Tournaisian (Taboada *et al.* 2019), and dropstones and glacially influenced soft-sediment deformation in the mid-Tournaisian Waaipoort Formation of South Africa (Streel and Theron 1999; Evans 2005, 1999; Lakin *et al.* 2016) indicate further glacigenic deposits elsewhere in Gondwana.

The record of glacial diamictites in the Agua de Lucho Formation increases the number of positively identified glacial records and extents the glaciated area in Gondwana. However, it is difficult to consider that these three regions were related to a single ice sheet, since the Argentinian glacial records were *c.* 3500 km away from the Brazilian, and *c.* 2500 km from those in South Africa (Fig. 10), and a single ice sheet would imply a much larger glaciated area than expected based on glacial eustasy (Rygel *et al.* 2008). It is more probable that at least a few glacial caps were present during this glacial interval. Despite being a distance apart, all three glaciated regions occurred at a minimum of 60° S palaeolatitude (Van Hinsbergen *et al.* 2015). This could suggest that ice caps were restricted to high latitude regions, in contrast to later Pennsylvanian–Permian ice caps which were usually located away from the South Pole (Montañez and Poulsen 2013).

The hierarchical structure of Mississippian climatic variability in western Argentina

In the last ten years, the LPIA has been interpreted as numerous ice centres of variable size that waxed and waned diachronically across Gondwana (e.g. Montañez and Poulsen 2013), causing a complex temporal dynamic characterized by the development of asynchronous glacial intervals (1–8 myr long) separated by non-glacial intervals (Fielding *et al.* 2008*a*, 2008*b*). Further shorter climatic

fluctuations are present within glacial intervals, indicating short-term advances and retreats of local glaciers and generating a stratigraphic pattern termed nested cyclicity by Birgenheier *et al.* (2009).

For the Mississippian of South America, Caputo *et al.* (2008) put forward a framework with two distinct glacial intervals, one in the middle Tournaisian and the other in the middle Visean. A mid-Visean glaciation has already been confirmed in western Argentina after diamictites from the top of the Cortaderas Formation were biostratigraphically constrained (Perez Loinaze 2007; Perez Loinaze *et al.* 2010), and glacial deposits from the Punta del Agua Formation (Báez *et al.* 2014) have been radiometrically dated at 335.9 ± 0.06 Ma (Gulbranson *et al.* 2010). However, this glaciation has been related to the classical late Serpukhovian–early Bashkirian glacial event recorded across the basin (López Gamundí and Martínez 2000; Henry *et al.* 2008; Dykstra *et al.* 2006) as a single protracted glacial episode lasting >10 myr and punctuated by an interglacial event (Limarino *et al.* 2014).

The glacial record in S1 to S6 in the Agua de Lucho Formation underscores the development of at least one other glacial event in western Argentina. This glacial event can probably be recognized in other localities, since putative Tournaisian diamictites have previously been described by Pazos (2007) in the Malimán Formation. The lack of evidence of ice activity in sequences 7–15 suggests the demise of glacial conditions. The presence of occasionally striated and faceted clasts in the conglomerate sequences of Cerro Tres Cóndores Formation (S14 and S15) suggests that they could be the result of reworked glacial deposits. Similarly, at the base of the Del Ratón Formation (late Tournaisian–early Visean), Milana and di Pasquo (2019) observed striated clasts which they interpreted as being inherited from a previous glacial cycle which is not preserved in this Formation.

It could be argued that a single, protracted glacial stage developed in western Argentina, starting at the Tournaisian and lasting until the Bashkirian, with records of several internal interglacial episodes. However, given the temporal scale involved in such climatic

Fig. 10. Palaeogeographic map for the studied interval (*c.* 350 Ma) showing the location of glaciated regions during the middle Tournaisian across Gondwana. (A) Agua de Lucho Formation (Río Blanco Basin, Argentina), (B) Poti Formation (Parnaíba Basin, Brazil) and (C) Waaiport Formation, Witteberg Group (Karoo Basin, South Africa). Modified from the plate motion model of Torsvik *et al.* (2012).

cyclicity (>20 myr), it is more reasonable to interpret an alternation of glacial–non-glacial intervals, similar to those developed during the Pennsylvanian–Permian of eastern Australia (Fielding *et al.* 2008*a*, 2008*b*).

Following this model, our data suggest the development of two glacial intervals in the Mississippian (middle Tournaisian and middle Visean, Fig. 9), in addition to the well-known late Serpukhovian–early Bashkirian. Each of these are separated by stratigraphic intervals that lack proximal ice evidence, interpreted as non-glacial intervals. This result implies the recognition, in western Argentina, of the Mississippian glacial events described by Caputo *et al.* (2008) in northern Brazil.

Previous descriptions of the mid-Tournaisian glacial records did not focus on internal variability, related to the waxing and waning of glaciers (Caputo *et al.* 2008; Playford *et al.* 2012). Sequence stratigraphic analyses have also failed to recognize internal cyclicity within these deposits (Lobato and Borghi 2014). Consequently, the idea of a single advance and retreat of glaciers was implicit for this interval. However, the sequence stratigraphic analysis of the Agua de Lucho Formation showed the presence of several glaciomarine cycles responding to the local advance and retreat of glaciers. Such stratigraphic cyclicity indicates several episodes of glacial maxima and minima within a single myr-scale glacial interval. This suggests that a complex hierarchy of climatic variability occurred during the Tournaisian of western Argentina, from myr glacial to non-glacial cycles to sub-myr cycles of glacial advance and retreat. Short-frequency climatic variability within longer glacial to non-glacial alterations conforms to the idea of nested cyclicity described by Birgenheier *et al.* (2009). Thus, the glacial to non-glacial framework and the nested cyclicity pattern defined by Birgenheier *et al.* (2009) and Fielding *et al.* (2008*a*, 2008*b*) can now be extended temporally to the early stages of the LPIA, and geographically to the western margin of Gondwana.

Conclusions

The *c*. 1400 m-thick succession of the Angualasto Group in the Río Blanco Basin, Argentina, is one of the best stratigraphic records of the Tournaisian in southwestern Gondwana, and reflects the regional palaeoclimatic evolution during this period of the LPIA.

In southern Sierra de Las Minitas, studied here for the first time, two detailed stratigraphic sections were carried out, including the basal glaciomarine Agua de Lucho Formation and the basal deposits of the overlying fan-deltaic Cerro Tres Cóndores Formation.

Sixteen siliciclastic lithofacies are recognized, ranging from diamictites, conglomerates, texturally mature sandstones, mixed sandstones and mudstones with dispersed gravel, through to bioturbated and fossiliferous mudstones and associated lithologies. Seven facies associations are interpreted, recording a variety of marine, glaciomarine and at times fan-deltaic environments. Lithofacies are arranged in depositional sequences that record relative sea-level variations associated to tectonism and glacial advance–retreat cycles. Three types of depositional sequences are recognized, and although the trend is not monotonic, these are interpreted as recording extensional settings with varying degrees of glacial influence at the base of the section, to no glacial influence at the top. Clast conglomerate composition, palaeocurrent measurements and detrital zircon age spectra suggest a source area in the Sierras Pampeanas basement, indicating relief formation and sediment supply from the east. Palaeontological and geochronological data indicate that the *c*. 1400 m-thick studied section was deposited from the middle to late Tournaisian.

Glacial sequences in the basal half of the Agua de Lucho Formation highlight the development of at least one other Mississippian (Tournaisian) glacial event located in western Argentina. It could be argued that it was part of a single protracted

glacial stage (Tournaisian to Bashkirian), with records of internal interglacial episodes. However, given the temporal climatic cyclicity involved (>10 myr), we suggest that it is an alternation of glacial to non-glacial intervals, similar to those developed during the Pennsylvanian–Permian of eastern Australia (Fielding *et al.* 2008*a*, 2008*b*). Current data for this region of Gondwana support the development of three glacial intervals, namely a middle Tournaisian, a middle Visean and a late Serpukhovian–Bashkirian. Each of these glacial episodes is limited by stratigraphic intervals that lack any evidence of proximal ice. This result implies the recognition, in western Argentina, of the Mississippian glacial events described by Caputo *et al.* (2008) for northern Brazil.

Previous descriptions of mid-Tournaisian glacial records in other regions of Gondwana did not recognize internal cyclicity within these deposits (Caputo *et al.* 2008; Playford *et al.* 2012; Lobato and Borghi 2014), suggesting a single episode of ice advance and retreat for this glacial period. However, our sequence stratigraphic analysis shows a complex hierarchical climatic variability with local advance and retreat of ice within a single myr scale, to sub-myr cycles. This indicates that the nested cyclicity pattern suggested for glacial records from other regions of Gondwana (Fielding *et al.* 2008*a*, 2008*b*; Birgenheier *et al.* 2009) could be extended temporally and geographically to the early stages of the LPIA and to the western margin of this supercontinent.

The shallowing-upward succession at the top of this section suggests the exhumation and development of local relief to the east from 350 Ma, and two alternatives could be considered as the trigger: the first is related to a global sea-level fall associated with the development of an ice cap in northern Gondwana at the Tournaisian–Visean boundary (Lees 1997; Bábek *et al.* 2013; Poty 2016); and the second is an isostatic rebound by lithospheric/crustal thinning in line with geological evidence and models reported or proposed for this region of Gondwana (Dávila *et al.* 2016; Martina *et al.* 2018).

The provenance analysis of the Cerro Tres Cóndores Formation suggests that Protoprecordillera would not have been a relevant source at this time, at least in this region. On the contrary, it would have constituted a bypass zone for sediments coming from the east. This is contrary to the hypothesis that the Agua de Lucho and Cerro Tres Cóndores formations represent synorogenic deposits as a result of the uplifting of the Protoprecordillera (Limarino *et al.* 2017).

Author contributions **ME**: conceptualization (lead), formal analysis (lead), investigation (lead), writing – original draft (lead), writing – review & editing (lead); **JJR**: funding acquisition (lead), investigation (equal), resources (lead), writing – original draft (equal); **DB**: conceptualization (equal), formal analysis (equal), investigation (equal), supervision (equal), writing – original draft (equal); **FMD**: conceptualization (lead), writing – review & editing (lead); **NEV**: conceptualization (equal), formal analysis (lead), funding acquisition (equal); **JAD**: data curation (lead), investigation (equal); **AS**: data curation (equal), investigation (equal); **GC**: data curation (equal), investigation (equal); **CP**: data curation (equal), investigation (equal); **MB**: data curation (equal)

Data availability statement All data generated or analysed during this study are included in this published article (and its supplementary information files).

Scientific editing by Adrian Hartley

References

Álvarez, J., Mpodozis, C. *et al.* 2011. Detrital zircons from late Paleozoic accretionary complexes in north-central Chile (28–32 S): possible fingerprints of the Chilenia terrane. *Journal of South American Earth Sciences*, **32**, 460–476, https://doi.org/10.1016/j.jsames.2011.06.002

Amos, A.J. 1958. Some Lower Carboniferous brachiopodsfrom the Volcan Formation, San Juan, Argentina. *Journal of Paleontology*, **32**, 838-845.

Amos, A.J. 1964. A review of the marine Carboniferous stratigraphy of Argentina. *In*: Proceeding 22 International Geological Congress, 53–72.

Astini, R.A., Dávila, F.M. *et al.* 2005. Cuencas de la región precordillerana. *In*: Chebli, G.A., Cortiñas, J.S. and Spalletti, L.A. (eds) *Frontera Exploratoria de La Argentina*. Instituto Argentino del Petróleo y del Gas, Buenos Aires, Argentina, 115–146.

Astini, R.A., Martina, F. and Dávila, F.M. 2011. La Formación Los Llantenes en la Precordillera de Jagüe (La Rioja) y la identificación de un episodio de extensión en la evolución temprana de las cuencas del Paleozoico superior en el oeste argentino. *Andean Geology*, **38**, 245–267, https://doi.org/10.5027/andgeoV38n2-a01

Astini, R.A., Martina, F., Ezpeleta, M., Dávila, F.M. and Cawood, P.A. 2009. Chronology from rifting to foreland basin in the Paganzo Basin (Argentina), and a reapprisal on the 'Eo- and Neohercynian' tectonics along Western Gondwana. *In*: *XII Congreso Geológico Chileno*. Chile, **S9-010**, Santiago, 40–43.

Azcuy, C.L. and Carrizo, H.A. 1995. Archaeosigillaria conferta (Carbonífero Temprano) en el Bolson de Jague, La Rioja, Argentina. *Ameghiniana*, **32**, 279–286.

Azcuy, C.L., Carrizo, H.A. and Caminos, R. 1999. Carbonífero y Pérmico de las Sierras Pampeanas, Famatina, Precordillera, Cordillera Frontal y Bloque de San Rafael. *In*: Caminos, R. (ed.) *Geología Argentina*. Instituto de Geología y Recursos Minerales, Buenos Aires, Argentina, 261–318.

Bábek, O., Kalvoda, J., Cossey, P., Šimíček, D., Devuyst, F.-X. and Hargreaves, S. 2013. Facies and petrophysical signature of the Tournaisian/Viséan (Lower Carboniferous) sea-level cycle in carbonate ramp to basinal settings of the Wales-Brabant massif, British Isles. *Sedimentary Geology*, **284**, 197–213, https://doi.org/10.1016/j.sedgeo.2012.12.008

Báez, W., Astini, R.A., Ezpeleta, M. and Martina, F. 2014. Facies volcaniclásticas y paleoambiente sedimentario de laFormación Punta del Agua, Carbonífero Temprano de la Precordillera Septentrional, La Rioja. *Revista de la Asociación Geológica Argentina*, **71**, 210–232.

Bann, K.L. and Fielding, C.R. 2004. An integrated ichnological and sedimentological comparison of non-deltaic shoreface and subaqueous delta deposits in Permian reservoir units of Australia. *Geological Society, London, Special Publications*, **228**, 273–310, https://doi.org/10.1144/GSL.SP.2004.228.01.13

Birgenheier, L.P., Fielding, C.R., Rygel, M.C., Frank, T.D. and Roberts, J. 2009. Evidence for Dynamic Climate Change on Sub-10^6-Year Scales from the Late Paleozoic Glacial Record, Tamworth Belt, New South Wales, Australia. *Journal of Sedimentary Research*, **79**, 56–82, https://doi.org/10.2110/jsr.2009.013

Borrello, A. 1955. Los conglomerados del Cerro Punta Negra, al oeste de Jagüé. *Revista de la Asociación Geológica Argentina*, **10**, 46–53.

Brezinski, D.K., Cecil, C.B., Skema, V.W. and Stamm, R. 2008. Late Devonian glacial deposits from the eastern United States signal an end of the mid-Paleozoic warm period. *Palaeogeography, Palaeoclimatology, Palaeoecology*, **268**, 143–151. https://doi.org/10.1016/j.palaeo.2008.03.042

Brezinski, D.K., Cecil, C.B. and Skema, V.W. 2010. Late Devonian glacigenic and associated facies from the central Appalachian Basin, eastern United States. *GSA Bulletin*, **122**, 265–281, https://doi.org/10.1130/B26556.1

Buggisch, W., Joachimski, M.M., Sevastopulo, G. and Morrow, J.R. 2008. Mississippian δ13Ccarb and conodont apatite δ18O records — Their relation to the Late Palaeozoic Glaciation. *Palaeogeography, Palaeoclimatology, Palaeoecology*, **268**, 273–292. https://doi.org/10.1016/j.palaeo.2008.03.043

Caminos, R., Fauqué, L. and Limarino, C. 1990. Las fases diastróficas intracarboníferas de la Precordillera y su correlación regional. *In*: *Late Paleozoic of South America*, Annual Meeting Working Group project IUGS 211, Abstracts, Buenos Aires. 132–146.

Caputo, M.V., de Melo, J.H.G., Streel, M. and Isbell, J.L. 2008. Late Devonian and Early Carboniferous glacial records of South America. *In*: Fielding, C.R., Frank, T.D. and Isbell, J.L. (eds) *Resolving the Late Paleozoic Ice Age in Time and Space*. Geological Society of America Special Papers 441, 161–173. https://doi.org/10.1130/2008.2441(11)

Cardozo, N. and Allmendinger, R.W. 2013. Spherical projections with OSXStereonet. *Computers & Geosciences*, **51**, 139–205, https://doi.org/10.1016/j.cageo.2012.07.021

Carrera, M.G., Rustán, J.J., Vaccari, N.E. and Ezpeleta, M. 2018. A new Mississippian hexactinellid sponge from the western Gondwana: Taxonomic and paleobiogeographic implications. *Acta Palaeontologica Polonica*, **63**, 63–70, https://doi.org/10.4202/app.00403.2017

Carrizo, H.A. and Azcuy, C.L. 1998. El perfil del cerro Mudadero y su flora fósil. Bolsón de Jagüé, Provincia de La Rioja. Argentina. *Acta Geológica Lilloana*, **18**, 81–99.

Carrizo, H.A. and Azcuy, C.L. 2015. Floras Neodevónicas-Eocarboníferas de Argentina. *Opera Lilloana*, **49**, 1–292.

Casquet, C., Pankhurst, R.J. *et al.* 2005. Grenvillian massif-type anorthosites in the Sierras Pampeanas. *Journal of the Geological Society*, **162**, 9–12, https://doi.org/10.1144/0016-764904-100

Catuneanu, O. 2017. Sequence Stratigraphy: Guidelines for a Standard Methodology. *In*: Montenari, M.B.T.-S. (eds) *Advances in Sequence Stratigraphy*. Academic Press, 1–57. https://doi.org/10.1016/bs.sats.2017.07.003

Catuneanu, O. and Zecchin, M. 2013. High-resolution sequence stratigraphy of clastic shelves II: controls on sequence development. *Marine and Petroleum Geology*, **39**, 26–38, https://doi.org/10.1016/j.marpetgeo.2012.08.010

Catuneanu, O., Abreu, V. *et al.* 2009. Towards the standardization of sequence stratigraphy. *Earth-Science Reviews*, **92**, 1–33. https://doi.org/10.1016/j.earscirev.2008.10.003

Catuneanu, O., Galloway, W.E., Kendall, C.G.S.C., Miall, A.D., Posamentier, H.W., Strasser, A. and Tucker, M.E. 2011. Sequence Stratigraphy: Methodology and Nomenclature. *Newsletters on Stratigraphy*, **44**, 173–245. https://doi.org/10.1127/0078-0421/2011/0011

Cisterna, G.A. 2011. Morphology and systematics of Late Palaeozoic syringothyrid brachiopods from West-Central Argentina. *Memoirs of the Association of Australasian Palaeontologists*, **41**, 315–325.

Cisterna, G.A. and Isaacson, P.E. 2003. A new Carboniferous brachiopod genus from South America. *Alcheringa*, **27**, 63–73. https://doi.org/10.1080/03115510308619545

Clark, J.A. and Primus, J.A. 1987. Sea-level changes resulting from future retreat of ice sheets: An effect of CO2 warming of the climate. In: Tooley, M.J. and Shennan, I. (eds), Sea-Level Changes. London, Institute of British Geography, 356–370.

Clifton, H.E. 2007. A reexamination of facies models for clastic shorelines. *In*: Posamentier, H.W. and Walker, H.W. (eds) *Facies Models Revisited*. SEPM Special Publication, **84**, 293–337.

Coira, B., Cisterna, C.E., Ulbrich, H.H. and Cordani, U.G. 2016. Extensional Carboniferous magmatism at the western margin of Gondwana: Las Lozas valley, Catamarca, Argentina. *Andean Geology*, **43**, 105–126, https://doi.org/10.5027/andgeoV43n1-a06

Collins, W. J. 2002. Nature of extensional accretionary orogens, Tectonics, **21**, https://doi.org/10.1029/2000TC001272

Collo, G., Astini, R.A., Cardona, A., Do Campo, M.D. and Cordani, U. 2008. Edades de metamorfismo en las unidades con bajo grado de la región central del Famatina: la impronta del ciclo orogénico oclóyico (Ordovícico). *Revista Geológica de Chile*, **35**, 191–213, https://doi.org/10.4067/S0716-02082008000200001

Conrad, C.P. 2013. The solid Earth's influence on sea level. *Geological Society of America Bulletin*, **125**, 1027–1052. https://doi.org/10.1130/B30764.1

Coughlin, T.J. 2000. *Linked Origen-Oblique Fault Zones in the Central Argentine Andes: The Basis for a New Model for Andean Orogenesis and Metallogenesis*. Queensland University.

Crowley, T.J. and Baum, S.K. 1991. Estimating Carboniferous sea-level fluctuations from Gondwanan ice extent. *Geology*, **19**, 975–977, https://doi.org/10.1130/0091-7613(1991)019<0975:ECSLFF>2.3.CO;2

Daemon, R. F. 1974. Palinomorfos-guias do Devoniano Superior e Carbonífero Inferior das bacias do Amazonas e Parnaíba. *Anais da Academia Brasileira de Ciências*,**46**, 549–587.

Dahlquist, J.A., Pankhurst, R.J. *et al.* 2013. Hf and Nd isotopes in Early Ordovician to Early Carboniferous granites as monitors of crustal growth in the Proto-Andean margin of Gondwana. *Gondwana Research*, **23**, 1617–1630, https://doi.org/10.1016/j.gr.2012.08.013

Dahlquist, J.A., Alasino, P.H., Basei, M.A.S., Cámera, M.M.M., Grande, M.M. and Neto, M.d.C.C. 2018*a*. Petrological, geochemical, isotopic, and geochronological constraints for the Late Devonian–Early Carboniferous magmatism in SW Gondwana (27–32° LS): an example of geodynamic switching. *International Journal of Earth Sciences*, **107**, 2575–2603, https://doi.org/10.1007/s00531-018-1615-9

Dahlquist, J.A., Alasino, P.H., Basei, M.A.S., Cámera, M.M.M., Grande, M.S.M., Neto, M.d.C.C. and Larrecharte, M.G. 2018*b*. Recurrent intrusive episodes in the Paleozoic metasedimentary upper crust during the Early Carboniferous time: The Veladero granitoid stock and the peraluminous andesite. *Journal of South American Earth Sciences*, **88**, 80–93, https://doi.org/10.1016/j.jsames.2018.08.011

Dalrymple, R.W., Mackay, D.A., Ichaso, A.A. and Choi, K.S. 2012. Processes, morphodynamics, and facies of tide-dominated estuaries. *In*: *Principles of Tidal Sedimentology*. Springer, 79–107.

Dávila, F., Martina, F. and Ávila, P. 2017. Mississippian glaciation in western Gondwana driven by mantle interaction. *In*: *XX Congreso Geológico Argentino*. San Miguel de Tucumán, 77–79.

Davis, J.L. and Mitrovica, J.X. 1996. Glacial isostatic adjustment and the anomalous tide gauge record of eastern North America. *Nature*, **379**, 331–333, https://doi.org/10.1038/379331a0

DeCelles, P.G., Langford, R.P. and Schwartz, R.K. 1983. Two new methods of paleocurrent determination from trough cross-stratification. *Journal of Sedimentary Research*, **53**, 629–642.

DeCelles, P.G., Gray, M.B., Ridgway, K.D., Cole, R.B., Pivnik, D.A., Pequera, N. and Srivastava, P. 1991. Controls on synorogenic alluvial-fan architecture, Beartooth Conglomerate (Palaeocene), Wyoming and Montana. *Sedimentology*, **38**, 567–590, https://doi.org/10.1111/j.1365-3091.1991.tb01009.x

Dietrich, P., Ghienne, J.-F., Lajeunesse, P., Normandeau, A., Deschamps, R. and Razin, P. 2018. Deglacial sequences and glacio-isostatic adjustment: Quaternary compared with Ordovician glaciations. *In*: Le Heron, D.P., Hogan, K.A., Phillips, E.R., Huuse, M., Busfield, M.E. and Graham, A.G.C. (eds) *Glaciated Margins: The Sedimentary and Geophysical Archive*. Geological Society, Special Publications, London, 475, 149–180. https://doi.org/10.1144/SP475.9

Dykstra, M., Kneller, B. and Milana, J.P. 2006. Deglacial and postglacial sedimentary architecture in a deeply incised paleovalley-paleofjord–The Pennsylvanian (late Carboniferous) Jejenes Formation, San Juan, Argentina. *Geological Society of America Bulletin*, **118**, 913–937. https://doi.org/10.1130/B25810.1

Evans, F.J. 1999. Palaeobiology of Early Carboniferous lacustrine biota of the Waaipoort Formation (Witteberg Group), South Africa. *Palaeontologia Africana*, **35**, 1–6. https://doi.org/10.1016/B978-1-4557-3143-5.00008-0

Evans, F.J. 2005. *Taxonomy, Palaeoecology and Palaeobiogeography of Some Palaeozoic Fish of Southern Gondwana*. University of Stellenbosch.

Eyles, C.H., Eyles, N. and Miall, A.D. 1985. Models of glaciomarine sedimentation and their application to the interpretation of ancient glacial sequences. *Palaeogeography, Palaeoclimatology, Palaeoecology*, **51**, 15–84, https://doi.org/10.1016/0031-0182(85)90080-X

Ezpeleta, M. 2009. *El Paleozoico Superior de La Región Central Del Famatina: Un Enfoque Tectosedimentario*. Universidad Nacional de Córdoba.

Ezpeleta, M. and Astini, R.A. 2008. *Labrado y relleno de un paleovalle glacial en la base de la Formación Río del Peñón (Carbonífero Superior), Precordillera Septentrional*. *In*: Simposio Argentino Del Paleozoico Superior.

Farrell, W.E. and Clark, J.A. 1976. On postglacial sea level. *Geophysical Journal of the Royal Astronomical Society*, **46**, 3, 647–667, https://doi.org/10.1111/j.1365-246X.1976.tb01252.x

Fauqué, L. and Limarino, C.O. 1991. El Carbonífero de Agua de Carlos (Precordillera de La Rioja), su importancia tectónica y paleoambiental. *Revista de la Asociación Geológica Argentina*, **46**, 103–114.

Fernández-Seveso, F. and Tankard, A.J. 1995. Tectonics and Stratigraphy of the Late Paleozoic Paganzo Basin of Western Argentina and its Regional Implications. *In*: Tankard, A.J., Soruco, R.S. and Welsink, H.J. (eds) *Petroleum Basins of South America*, American Association of Petroleum Geologists, Memoirs, Tulsa, OK, **62**, 285–301. https://doi.org/10.1306/M62593C13

Fielding, C.R. 2018. Stratigraphic architecture of the Cenozoic succession in the McMurdo Sound region, Antarctica: An archive of polar palaeoenvironmental change in a failed rift setting. *Sedimentology*, **65**, 1–61. https://doi.org/10.1111/sed.12413

Fielding, C.R., Frank, T.D., Birgenheier, L.P., Rygel, M.C., Jones, A.T. and Roberts, J. 2008*a*. Stratigraphic imprint of the Late Palaeozoic Ice Age in eastern Australia: a record of alternating glacial and nonglacial climate regime. *Journal of the Geological Society*, **165**, 129–140, https://doi.org/10.1144/0016-76492007-036

Fielding, C.R., Frank, T.D., Birgenheier, L.P., Rygel, M.C., Jones, A.T. and Roberts, J. 2008*b*. Stratigraphic record and facies associations of the late Paleozoic ice age in eastern Australia (New South Wales and Queensland). *In*: Fielding, C.R., Frank, T.D. and Isbell, J.L. (eds) *Resolving the Late Paleozoic Ice Age in Time and Space*. Geological Society of America Special Papers, **441**, 41–57. https://doi.org/10.1130/2008.2441(03)

Frank, T.D., Birgenheier, L.P. *et al.* 2008. Late Paleozoic climate dynamics revealed by comparison of ice-proximal stratigraphic and ice-distal isotopic records. *In*: *Resolving the Late Paleozoic Ice Age in Time and Space*. Geological Society of America Special Papers, **441**, 331–342. https://doi.org/10.1130/2008.2441(23)

Gallastegui Suárez, G., González Menéndez, L., Rubio Ordóñez, Á, Cuesta Fernández, A. and Gerdes, A. 2014. Origin and provenance of igneous clasts from late Palaeozoic conglomerate formations (Del Ratón and El Planchón) in the Andean Precordillera of San Juan, Argentina. *Journal of Iberian Geology*, 261–282, http://doi.org/10.5209/rev_JIGE.2014.v40.n2.45298

Giles, P.S. 2012. Low-latitude Ordovician to Triassic brachiopod habitat temperatures (BHTs) determined from δ18O [brachiopod calcite]: A cold hard look at ice-house tropical oceans. *Palaeogeography, Palaeoclimatology, Palaeoecology*, **317–318**, 134–152. https://doi.org/10.1016/j.palaeo.2012.01.002

González, C.R. 1985. Esquema bioestratigráfico del Paleozoico Superior marino de la Cuenca Uspallata-Iglesia, República Argentina. *Acta Geológica Lilloana*, **16**, 231–244.

González, C.R. 1994. Early Carboniferous Bivalvia from Western Argentina. *Alcheringa*, **18**, 169–185, https://doi.org/10.1080/03115518.1994.9638775

González, C.R. and Bossi, G.E. 1986. Los depósitos carbónicos al oeste de Jagüel, La Rioja. *In*: *IV Congreso Argentino de Paleontología y Bioestratigrafía*, Mendoza, Argentina, 231–236.

González, C.R. and Bossi, G.E. 1987. Descubrimiento del Carbonífero inferior marino al oeste de Jagüé, La Rioja. I:IV *Congreso Latinoamericano de Paleontología*. Santa Cruz de La Sierra, Bolivia, 713-724.

Gulbranson, E.L., Montañez, I.P., Schmitz, M.D., Limarino, C.O., Isbell, J.L., Marenssi, S.A. and Crowley, J.L. 2010. High-precision U-Pb calibration of Carboniferous glaciation and climate history, Paganzo Group, NW Argentina. *Geological Society of America Bulletin*, **122**, 1480–1498. https://doi.org/10.1130/B30025.1

Gulbranson, E.L., Isbell, J.L., Montañez, I.P., Limarino, C.O., Marenssi, S.A., Meyer, K. and Hull, C. 2014. Reassessment of mid-Carboniferous glacial extent in southwestern Gondwana (Rio Blanco Basin, Argentina) inferred from paleo-mass transport of diamictites. *Gondwana Research*, **25**, 1369–1379. https://doi.org/10.1016/j.gr.2013.03.017

Gutiérrez, P.R. and Limarino, C.O. 2006. El perfil del sinclinal del Rincon Blanco (noroeste de La Rioja): El limite Carbonifero-Permico en el noroeste Argentino. *Ameghiniana*, **43**, 687–703.

Harrison, C.G.A. 1990. Long-term eustasy and epeirogeny in continents, *In*: Revelle, R.R. (ed.) *Sea-Level Change*. National Academy Press, Washington, D.C., 141–158.

Henry, L.C., Isbell, J.L. and Limarino, C.O. 2008. Carboniferous glacigenic deposits of the proto-Precordillera of west-central Argentina. *In*: Fielding, C.R., Frank, T.D. and Isbell, J.L. (eds) *Resolving the Late Paleozoic Ice Age in Time and Space*. Geological Society of America Special Papers, **441**, 131–142. https://doi.org/10.1130/2008.2441(09)

Howard, J.L. 1993. The statistics of counting clasts in rudites: a review, with examples from the upper Palaeogene of southern California, USA. *Sedimentology*, **40**, 157–174, https://doi.org/10.1111/j.1365-3091.1993.tb01759.x

Iannizzotto, N.F., Rapela, C.W., Baldo, E.G.A., Galindo, C., Fanning, C.M. and Pankhurst, R.J. 2013. The Sierra Norte-Ambargasta batholith: Late Ediacaran–Early Cambrian magmatism associated with Pampean transpressional tectonics. *Journal of South American Earth Sciences*, **42**, 127–143, https://doi.org/10.1016/j.jsames.2012.07.009

Isaacson, P.E. and Dutro, J.T. 1999. Lower Carboniferous brachiopods from Sierra de Almeida, northern Chile. *Journal of Paleontology*, **73**, 625–633, https://doi.org/10.1017/S0022336000032443

Isaacson, P.E., Diaz-Martinez, E., Grader, G.W., Kalvoda, J., Babek, O. and Devuyst, F.X. 2008. Late Devonian-earliest Mississippian glaciation in Gondwanaland and its biogeographic consequences. *Palaeogeography, Palaeoclimatology, Palaeoecology*, **268**, 126–142, https://doi.org/10.1016/j.palaeo.2008.03.047

Isbell, J.L., Miller, M.F., Wolfe, K.L. and Lenaker, P.A. 2003. Timing of late Paleozoic glaciation in Gondwana: Was glaciation responsible for the development of Northern Hemisphere cyclothems? *Geological Society of America Special Papers*, **370**, 5–24. https://doi.org/10.1130/0-8137-2370-1.5

Johnson, H.D., Baldwin, C.T. and Reading, H.G. 2002. Shallow Clastic Seas. *In*: *Sedimentary Environments: Processes, Facies, and Stratigraphy*. Blackwell Science, Oxford, 232–279.

Kammer, T.W. and Matchen, D.L. 2008. Evidence for eustasy at the Kinderhookian-Osagean (Mississippian) boundary in the United States: Response to late Tournaisian glaciation. *In*: Fielding, C.R., Frank, T.D. and Isbell, J.L. (eds) *Resolving the Late Paleozoic Ice Age in Time and Space*. Geological Society of America Special Papers, **441**, 261–274. https://doi.org/10.1130/2008.2441(18)

Kellerhals, P. and Matter, A. 2003. Facies analysis of a glaciomarine sequence, the Neoproterozoic Mirbat Sandstone Formation, Sultanate of Oman. *Eclogae Geologicae Helvetiae*, **96**, 49–70. https://doi.org/10.1007/S00015-003-1068-3

Lakin, J.A., Marshall, J.E.A., Troth, I. and Harding, I.C. 2016. Greenhouse to icehouse: a biostratigraphic review of latest Devonian–Mississippian glaciations and their global effects. *Geological Society, London, Special Publications*, **423**, 439–464. https://doi.org/10.1144/SP423.12

Lees, A. 1997. Biostratigraphy, sedimentology and palaeobathymetry of Waulsortian buildups and peri-Waulsortian rocks during the Late Tournaisian regression, Dinant area, Belgium. *Geological Journal*, **32**, 1–36, https://doi.org/10.1002/(SICI)1099-1034(199703)32:1<1::AID-GJ715>3.0.CO;2-0

Limarino, C.O. and Césari, S.N. 1993. Reubicación estratigráfica de la Formación Cortaderas y definición del Grupo Angualasto (Carbonífero Inferior, Precordillera de San Juan). *Revista de la Asociación Geológica Argentina*, **47**, 61–72.

Limarino, C.O. and Spalletti, L.A. 2006. Paleogeography of the upper Paleozoic basins of southern South America: An overview. *Journal of South American Earth Sciences*, **22**, 134–155, https://doi.org/10.1016/j.jsames.2006.09.011

Limarino, C.O., Tripaldi, A., Marenssi, S.A. and Fauqué, L. 2006. Tectonic, sea-level, and climatic controls on Late Paleozoic sedimentation in the western basins of Argentina. *Journal of South American Earth Sciences*, **22**, 205–226, https://doi.org/10.1016/j.jsames.2006.09.009

Limarino, C.O., Césari, S.N., Spalletti, L.A., Taboada, A.C., Isbell, J.L., Geuna, S.E. and Gulbranson, E. 2014. A paleoclimatic review of southern South America during the late Paleozoic: A record from icehouse to extreme greenhouse conditions. *Gondwana Research*, **25**, 1396–1421. https://doi.org/10.1016/j.gr.2012.12.022

Limarino, C.O., Schencman, L.J., Alonso Muruaga, P. and Césari, S.N. 2017. Análisis estratigráfico de las sequencias Neopaleozoicas de la Precordillera septentrional. *Revista de la Asociacion Geologica Argentina*, **74**, 449–467.

Lobato, G. and Borghi, L. 2014. Estratigrafia de sequências do contato formacional Longá/Poti (Carbonífero Inferior) em testemunhos de sondagem da Bacia do Parnaíba. *Boletim de Geociencias Petrobras*, **22**, 213–235.

Longhitano, S.G. 2011. The record of tidal cycles in mixed silici–bioclastic deposits: examples from small PlioPleistocene peripheral basins of the microtidal Central Mediterranean Sea. *Sedimentology*, **58**, 691–719, https://doi.org/10.1111/j.1365-3091.2010.01179.x

Lønne, I. 1995. Sedimentary facies and depositional architecture of ice-contact glaciomarine systems. *Sedimentary Geology*, **98**, 13–43, https://doi.org/10.1016/0037-0738(95)00025-4

López Gamundí, O.R. and Martínez, M. 2000. Evidence of glacial abrasion in the Calingasta–Uspallata and western Paganzo basins, mid-Carboniferous of western Argentina. *Palaeogeography, Palaeoclimatology, Palaeoecology*, **159**, 145–165. https://doi.org/10.1016/S0031-0182(00)00044-4

López Gamundí, O.R., Limarino, C.O. and Césari, S.N. 1992. Late Paleozoic paleoclimatology of central west Argentina. *Palaeogeography, Palaeoclimatology, Palaeoecology*, **91**, 305–329. https://doi.org/10.1016/0031-0182(92)90074-F

López Gamundí, O.R., Espejo, I.S., Conaghan, P.J. and Powell, C.M. 1994. Southern South America. *Geological Society of America, Memoir*, **1984**, 281–329, https://doi.org/10.1130/MEM184-p281

MacEachern, J.A. and Bann, K.L. 2008. The role of ichnology in refining shallow marine facies models. *In*: Hampson, G.J., Steel, R.J., Burgess, P.M. and Dalrymple, R.W. (eds) *Recent Advances in Models of Siliciclastic Shallow-Marine Stratigraphy*. SEPM Special Publication 90, Tulsa, USA, 73–116.

Martina, F. Viramonte, J.M., Astini, R.A., Pimentel, M.M. Dantas, E. 2011. Mississippian volcanism in the south-central Andes: New U-Pb SHRIMP zircon geochronology and whole-rock geochemistry. *Gondwana Research*, **19**, 524-534, https://doi.org/10.1016/j.gr.2010.07.004

Martina, F., Canelo, H.N., Dávila, F.M., de Hollanda, M.H.M. and Teixeira, W. 2018. Mississippian lamprophyre dikes in western Sierras Pampeanas, Argentina: Evidence of transtensional tectonics along the SW margin of Gondwana. *Journal of South American Earth Sciences*, **83**, 68–80, https://doi.org/10.1016/j.jsames.2018.02.006

Martins-Neto, M.A. and Catuneanu, O. 2010. Rift sequence stratigraphy. *Marine and Petroleum Geology*, **27**, 247–253, https://doi.org/10.1016/j.marpetgeo.2009.08.001

Matchen, D.L. and Kammer, T.W. 2006. Incised valley fill interpretation for Mississippian Black Hand Sandstone, Appalachian Basin, USA: Implications for glacial eustasy at Kinderhookian–Osagean (Tn2–Tn3) boundary. *Sedimentary Geology*, **191**, 89–113. https://doi.org/10.1016/j.sedgeo.2006.02.002

Miall, A.D. 1996. *The Geology of Fluvial Deposits, Sedimentary Facies, Basin Analysis and Petroleum Geology*. Springer-Verlag, New York, 668.

Milana, J.P. and Di Pasquo, M. 2019. New chronostratigraphy for a lower to upper Carboniferous strike-slip basin of W-Precordillera (Argentina): Paleogeographic, tectonic and glacial importance. *Journal of South American Earth Sciences*, **96**, https://doi.org/10.1016/j.jsames.2019.102383

Miller, K.G., Kominz, M.A. *et al.* 2005. The Phanerozoic record of global sea-level change. *Science*, **310**, 1293–1298, https://doi.org/10.1126/science.1116412

Milne, G.A. and Mitrovica, J.X. 2008. Searching for eustasy in deglacial sea-level histories. *Quaternary Science Reviews*, **27**, 2292–2302. https://doi.org/10.1016/j.quascirev.2008.08.018

McCarthy, P.J. and Plint, A.G. 1998. Recognition of interfluve sequence boundaries: integrating paleopedology and sequence stratigraphy. *Geology*, **26**, 387–390, https://doi.org/10.1130/0091-7613(1998)026<0387:ROISBI>2.3.CO;2

McGhee, G.R.J. 2018. *Carboniferous Giants and Mass Extinction. The Late Paleozoic Ice Age World*. Columbia University Press, New York.

Montañez, I.P. and Poulsen, C.J. 2013. The Late Paleozoic Ice Age: An Evolving Paradigm. *Annual Review of Earth and Planetary Sciences*, **41**, 629–656. https://doi.org/10.1146/annurev.earth.031228.100118

Mulder, T., Syvitski, J.P.M., Migeon, S., Faugeres, J.-C. and Savoye, B. 2003. Marine hyperpycnal flows: initiation, behavior and related deposits. A review. *Marine and Petroleum Geology*, **20**, 861–882, https://doi.org/10.1016/j.marpetgeo.2003.01.003

Mutti, E. 1992. *Turbidite Sandstones*. Agip, Istituto di geologia, Università di Parma.

Niemeyer, H., Urzua, F. and Rubinstein, C.V. 1997. Nuevos antecedentes estratigráficos y sedimentológicos de la Formación Zorritas, Devónico-Carbonífero de Sierra Almeida, Región de Antofagasta, Chile. *Revista Geológica de Chile*, **24**, 25–43.

Ogg, J.G., Ogg, G.M. and Gradstein, F.M. 2016. 8 - Devonian. *A Concise Geologic Time Scale*, 85–98. https://doi.org/10.1016/b978-0-444-59467-9.00008-x

Pazos, P.J. 2007. Cyclostratigraphy during the Carboniferous glaciations in central western Argentina: glacial ageism and tectonic framework. *In*: Milani, E.J., Iannuzzi, R., Chemale, F. and Frantz, J.C. (eds) *Problems in Western Gondwana Geology*. RGEOTEC – Rede de Estudos Geotectônicos, Gramado, Brazil, 108–114.

Pazos, P.J., Rusconi, F.J., Loss, M.L., Gutiérrez, C. and Heredia, A.M. 2017. Stratigraphy of the El Imperial formation (Pennsylvanian-cisuralian) in the Atuel Canyon, San Rafael basin. *Revista de la Asociacion Geologica Argentina*, **74**, 155-162.

Perez Loinaze, V.S. 2007. A Mississippian miospore biozone for Southern Gondwana. *Palynology*, **31**, 101–117. https://doi.org/10.2113/gspalynol.31.1.101

Perez Loinaze, V.S., Limarino, C.O. and Césari, S.N. 2010. Glacial events in Carboniferous sequences from Paganzo and Río Blanco Basins (Northwest Argentina): Palynology and depositional setting. *Geologica Acta*, **8**, 399–418. https://doi.org/10.1344/105.000001579

Playford, G. and Melo, J.H.G. 2010. Morphological variation and distribution of the Tournaisian (Early Mississippian) miospore Waltzispora lanzonii Daemon 1974. *Neues Jahrbuch für Geologie und Paläontologie - Abhandlungen*, **256**, 183–193. https://doi.org/10.1127/0077-7749/2010/0043

Playford, G., Borghi, L. and Lobato, G. 2012. Palynological dating and correlation of Early Mississippian (Tournaisian) diamictite sections, Parnaíba Basin, northeastern Brazil. *Revista Española de Micropaleontología*, **44**, 1–22.

Postma, G. 1990. Depositional architecture and facies of river and fan deltas: a synthesis. *In*: Colella, A. and Prior, D.B. (eds) *Coarse Grained Deltas*. Spec Publ. Int. Ass. Sediment, **10**, 13–27.

Potter, P.E. and Pettijohn, F.J. 1977. *Paleocurrents and Basin Analysis*. Springer-Verlag, Heidelberg.

Poty, E. 2016. The Dinantian (Mississippian) succession of southern Belgium and surrounding areas: stratigraphy improvement and inferred climate reconstruction. *Geologica Belgica*, **19**, 177–200, https://doi.org/10.20341/gb.2016.014

Powell, R.D. 1990. Glacimarine processes at grounding-line fans and their growth to ice-contact deltas. *Geological Society, London, Special Publications*, **53**, 53–73, https://doi.org/10.1144/GSL.SP.1990.053.01.03

Powell, R.D. and Cooper, J.M. 2002. A glacial sequence stratigraphic model for temperate, glaciated continental shelves. *Geological Society, London, Special Publications*, **203**, 215–244, https://doi.org/10.1144/GSL.SP.2002.203.01.12

Prestianni, C., Rustán, J.J. *et al.* 2015. Early seed plants from Western Gondwana: Paleobiogeographical and ecological implications based on Tournaisian (Lower Carboniferous) records from Argentina. *Palaeogeography, Palaeoclimatology, Palaeoecology*, **417**, 210–219. https://doi.org/10.1016/j.palaeo.2014.10.039

Rapela, C.W., Pankhurst, R.J. *et al.* 2007. The Rio de la Plata craton and the assembly of SW Gondwana. *Earth-Science Reviews*, **83**, 49–82, https://doi.org/10.1016/j.earscirev.2007.03.004

Rapela, C.W., Verdecchia, S.O. *et al.* 2016. Identifying Laurentian and SW Gondwana sources in the Neoproterozoic to Early Paleozoic metasedimentary rocks of the Sierras Pampeanas: Paleogeographic and tectonic implications. *Gondwana Research*, **32**, 193–212, https://doi.org/10.1016/j.gr.2015.02.010

Rosa, E.L.M., Vesely, F.F., Isbell, J.L., Kipper, F., Fedorchuk, N.D. and Souza, P.A. 2019. Constraining the timing, kinematics and cyclicity of Mississippian-Early Pennsylvanian glaciations in the Paraná Basin, Brazil. *Sedimentary Geology*, **384**, 29–49. https://doi.org/10.1016/j.sedgeo.2019.03.001

Rubinstein, C.V., Petus, E. and Niemeyer, H. 2017. Palynostratigraphy of the Zorritas Formation, Antofagasta region, Chile: Insights on the Devonian/Carboniferous boundary in western Gondwana. *Geoscience Frontiers*, **8**, 493–506. https://doi.org/10.1016/j.gsf.2016.04.005

Rustán, J.J., Vaccari, N.E. and Astini, R.A. 2011. Early Devonian Trilobites from the Sierra de las Minitas, Northernmost Precordillera (La Rioja Province), Argentina. *Ameghiniana*, **48**, 226–241, https://doi.org/10.5710/AMGH.v48i1(335)

Rygel, M.C., Fielding, C.R., Frank, T.D. and Birgenheier, L.P. 2008. The Magnitude of Late Paleozoic Glacioeustatic Fluctuations: A Synthesis. *Journal of Sedimentary Research*, **78**, 500–511. https://doi.org/10.2110/jsr.2008.058

Sabattini, N., Carrizo, H.A. and Azcuy, C.L. 2001. Invertebrados marinos de la Formación Malimán (Carbonífero Inferior), y su relación con las asociaciones paleoflorísticas. *Revista de la Asociación Geológica Argentina*, **56**, 111–120.

Saltzman, M.R. 2002. Carbon and oxygen isotope stratigraphy of the Lower Mississippian (Kinderhookian–lower Osagean), western United States: Implications for seawater chemistry and glaciation. *Geological Society of America Bulletin*, **114**, 96–108. https://doi.org/10.1130/0016-7606(2002)114<0096:CAOISO>2.0.CO;2

Saltzman, M.R. 2003. The late Paleozoic ice age; oceanic gateway or pCO2? *Geology*, **31**, 151–154. https://doi.org/10.1130/0091-7613(2003)031<0151:LPIAOG>2.0.CO;2

Scalabrini Ortiz, J. and Arrondo, O.G. 1973. Contribución al conocimiento del Carbónico de los perfiles del cerro Veladero y del río del Piñón (Precordillera de La Rioja). *Revista del Museo de La Plata*, **8**, 257–279.

Sterren, A.F. and Cisterna, G.A. 2010. Bivalves and brachiopods in the Carboniferous-Early Permian of Argentine Precordillera: Diversification and faunal turnover in Southwestern Gondwana. *Geologica Acta*, **8**, 501–517. https://doi.org/10.1344/105.000001585

Sterren, A.F., Cisterna, G.A., Rustán, J.J., Vaccari, N.E. and Ezpeleta, M. 2013. Nuevos registros de invertebrados marinos en las sedimentitas Devónico–Carboníferas de la Sierra De Las Minitas, Precordillera Septentrional de La Rioja, Argentina. *Ameghiniana*, **56 (S)**, R71.

Streel, M. and Theron, J.N. 1999. The Devonian-Carboniferous boundary in South Africa and the age of the earliest episode of the Dwyka glaciation: New palynological result. *Episodes*, **22**, 41–44, https://doi.org/10.18814/epiiugs/1999/v22i1/007

Taboada, A., Pagani, M., Pinilla, M., Tortello, F. and Taboada, C. 2019. Carboniferous deposits of northern Sierra de Tecka, central-western

M. Ezpeleta *et al.*

Patagonia, Argentina: paleontology, biostratigraphy and correlations. *Andean Geology*, **46**, 629–669. https://doi.org/10.5027/andgeoV46n3-3143

Torsvik, T.H., Van der Voo, R. *et al.* 2012. Phanerozoic polar wander, palaeogeography and dynamics. *Earth-Science Reviews*, **114**, 325–368. https://doi.org/10.1016/j.earscirev.2012.06.007

Vaccari, N.E., Rustán, J.J., Sterren, A.F., Cisterna, G.A., Ezpeleta, M. and Balseiro, D. 2013. Primer registro de Pudoproetus (Trilobita) en el Tournaisiano de la Formación Agua de Lucho, La Rioja, Argentina: significado bioestratigráfico. *Ameghiniana*, **50 (S)**, R74.

Van Hinsbergen, D.J.J., De Groot, L.V. *et al.* 2015. A paleolatitude calculator for palaeoclimate studies. *PLoS ONE*, **10**, 1–21. https://doi.org/10.1371/journal.pone.0126946

Veevers, J.J. and Powell, C.M. 1987. Late Paleozoic glacial in Gondwanaland reflected in trangressive-regressive depostional sequences in Euramerica. *Geological Society of America Bulletin*, **98**, 475–487, https://doi.org/10.1130/0016-7606(1987)98<475:LPGEIG>2.0.CO;2

Von Gosen, W., McClelland, W.C., Loske, W., Martinez, J.C. and Prozzi, C. 2014. Geochronology of igneous rocks in the Sierra Norte de Córdoba (Argentina): Implications for the Pampean evolution at the western Gondwana margin. *Lithosphere*, **6**, 277–300, https://doi.org/10.1130/L344.1

Wallace, Z. and Elrick, M. 2014. Early Mississippian orbital-scale glacio-eustasy detected from high-resolution oxygen isotopes of marine apatite (Conodonts). *Journal of Sedimentary Research*, **84**, 816–824, https://doi.org/10.2110/jsr.2014.69

Wicander, R., Clayton, G., Marshall, J.E.A., Troth, I. and Racey, A. 2011. Was the latest Devonian glaciation a multiple event? New palynological evidence from Bolivia. *Palaeogeography, Palaeoclimatology, Palaeoecology*, **305**, 75–83. https://doi.org/10.1016/j.palaeo.2011.02.016

Yao, L., Qie, W. *et al.* 2015. The TICE event: Perturbation of carbon-nitrogen cycles during the mid-Tournaisian (Early Carboniferous) greenhouse-ice-house transition. *Chemical Geology*, **401**, 1–14. https://doi.org/10.1016/j.chemgeo.2015.02.021

Zecchin, M., Caffau, M., Tosi, L., Civile, D., Brancolini, G., Rizzetto, F. and Roda, C. 2010. The impact of Late Quaternary glacio-eustasy and tectonics on sequence development: evidence from both uplifting and subsiding settings in Italy. *Terra Nova*, **22**, 324–329. https://doi.org/10.1111/j.1365-3121.2010.00953.x